Journal Pre-proof

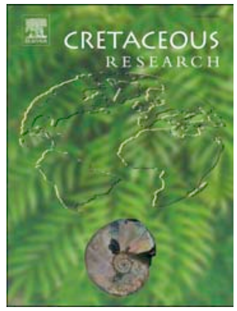

Multiproxy provenance analysis of Lower to Upper Cretaceous synorogenic deposits in the Southern Andes (34-35°S): evidence of coeval volcanism during the onset of the Andean orogeny

Ricardo Gómez, Antonella Galetto, Guadalupe Arzadún, Maisa Tunik, Silvio Casadio, Martin Parada, Lucas Lothari

PII: S0195-6671(21)00233-0

DOI: https://doi.org/10.1016/j.cretres.2021.104985

Reference: YCRES 104985

To appear in: *Cretaceous Research*

Received Date: 12 August 2020

Revised Date: 30 June 2021

Accepted Date: 25 July 2021

Please cite this article as: Gómez, R., Galetto, A., Arzadún, G., Tunik, M., Casadio, S., Parada, M., Lothari, L., Multiproxy provenance analysis of Lower to Upper Cretaceous synorogenic deposits in the Southern Andes (34-35°S): evidence of coeval volcanism during the onset of the Andean orogeny, *Cretaceous Research*, https://doi.org/10.1016/j.cretres.2021.104985.

Credit Author Statement

Ricardo Gómez: designed the research, provided lithological column information, collected the rock samples and wrote the paper with input from all authors.

Antonella Galetto: contributed to the discussion of fission track analysis.

Guadalupe Arzadún: performed fission track analysis.

Maisa Tunik: collected the rock samples and provided lithological column information.

Silvio Casadio: collected the rock samples and provided lithological column information.

Martin Parada: Prepared samples and photographs from SEM.

Lucas Lothari: collected the sediment samples and provided lithological column information

All authors discussed the results and commented on the final manuscript.

Multiproxy provenance analysis of Lower to Upper Cretaceous synorogenic deposits in the Southern Andes (34-35°S): evidence of coeval volcanism during the onset of the Andean orogeny

Ricardo Gómez[a,b]*, Antonella Galetto[b,c], Guadalupe Arzadún[b,d], Maisa Tunik[a,b], Silvio Casadio[a,b], Martin Parada[a], Lucas Lothari[b,e]

[a] Universidad Nacional de Río Negro. Instituto de Investigación en Paleobiología y Geología. Av. Roca 1242, General Roca, Río Negro, Argentina. E-mail: rgomez@unrn.edu.ar

[b] Consejo Nacional de Investigaciones Científicas y Técnicas (CONICET).

[c] CONICET-IDEAN, Universidad de Buenos Aires, Ciudad Universitaria, C1428EHA, Buenos Aires, Argentina.

[d] Laboratorio de Termocronología (LaTe Andes), Las Moreras 510, 4401 Vaqueros, Salta, Argentina.

[e] IANIGLA, CCT Mendoza, CONICET, Parque San Martín s/n, 5500, Mendoza, Argentina.

*Corresponding author e-mail: rgomez@unrn.edu.ar

Abstract

The combination of detrital low-temperature thermochronology with previous U-Pb geochronology, petrological and sedimentological analyses, has proven to be a valuable approach to constrain the provenance of non-marine Lower to Upper Cretaceous synorogenic deposits in the northern Neuquén Basin. This work focuses on the study of the Diamante Formation, a fluvial succession that represents the first synorogenic products of the Andean foreland basin at 34-35°S. The results indicate that the deposition of the Diamante Formation occurred simultaneously with the existence of an active western volcanic arc during the onset of the foreland basin. The facies associations evidence the transition between the backarc and the foreland basin stages as well as the inception of fluvial sedimentation in the foredeep. Petrographic analyses, together with changes in the paleocurrents and the record of limestone clasts suggest a regional detrital source shift. Apatite fission-track analyses (AFT) of a sample collected from the lower part of the Diamante Formation indicate an Albian central cooling age. This sample also evidences a remarkable presence of angular apatite and zircon crystals with subordinated rounded and subangular grains. Zircon fission-track analyses (ZFT) of a sample from the upper part of the Diamante Formation yield two discrete populations of cooling ages, both reflecting source-cooling during the Late Jurassic (~161 Ma) and the Permian (~265 Ma). Finally, a comparison between the AFT and the U-Pb maximum depositional zircon-age reveals a short lag time (ca. 3 ma), likely related to the rapid magmatic cooling of a coeval volcanic source at ~110 Ma (Albian).

Keywords: Foreland Basin; Fluvial succession; Diamante Formation; latest Early Cretaceous; Fission Track; U-Pb geochronology

1. Introduction

A combination of multiple techniques has been a useful tool to perform provenance studies in the last decade. The analysis of detrital crystals with particular chemical and isotopic signatures reveals associations with source areas and tectonic events in many geological scenarios (Carrapa et al., 2009; Carrapa, 2010; Cawood et al., 2012; Chew and Donelick, 2012; Peyton and Carrapa, 2013; Gehrels, 2014; Owusu Agyemang et al., 2019). The changes of the allocyclic and autocyclic processes that influence the sedimentation over time can generate sediments of variable compositions derived from a similar source or, conversely, very similar sedimentary rock derived from different sources. The recognition of different compositional patterns in the detrital components of sedimentary sequences allows for the identification of diverse source signals (Cecil, 2003; Tyrrell et al., 2012; Franklin et al., 2019). Additionally, combined geochronometry and low-temperature thermochronometry enhance the recognition of syntectonic provenance information, by providing crystallization and thermotectonic histories of the same source rocks feeding the basin (Malusá and Fitzgerald, 2019 and references therein). Multiproxy analysis, including multidating methods, is a powerful tool for the reconstruction of the tectonic history of foreland basin systems (Bernet and Spiegel, 2004; Umazano et al., 2009; Ghiglione et al., 2015; Suriano et al., 2017; Thomson et al., 2017; Buelow et al., 2018; Bernet, 2019 and references therein).

The Neuquén Basin (Fig. 1) is a large depocenter developed during Late Triassic to Paleogene times in the southwestern margin of Gondwana (30-40°S) created by continental-scale rifting processes in response to the break-up of the Pangea supercontinent (Mpodozis and Ramos, 2008; Charrier et al., 2015; D’Elia et al., 2020; among others), with the potential influence of upper-plate movement and basement fabrics interaction (Fennell et al., 2020 and references therein). It records a thick Mesozoic sedimentary sequence of more than 7.000 m including marine and non-marine sedimentary rocks. Between the Early to Late Cretaceous, the Neuquén Basin changed from a backarc extensional basin to a retroarc foreland basin, in response to a westward acceleration of the South American plate during the Cretaceous (Mpodozis and Ramos, 1990; Howell et al., 2005; Ramos and Kay, 2006; Tunik et al., 2010). Congruent with this tectonic setting, several large-scale drainage systems have been interpreted for the Upper Cretaceous non-marine deposits of the Neuquén Basin, based on stratigraphy and sedimentology (e.g., Di Giulio et al., 2012, 2017; Gómez et al., 2019, 2020). Provenance analyses in the northern part of the basin (34-35°S) suggest that the foreland basin began to form at approximately 100-107 Ma with the deposition of the Diamante Formation, which is temporally equivalent to the youngest formation of the Neuquén Group described south of 35°S (Fig. 1; Gómez et al., 2019, 2020). A proposed source rock-model includes a westward sediment dispersion derived from the Sierra Pintada System and the San Rafael Block before the uplift of the Andes, which was then shifted eastwards with the onset of the Andean orogeny, associated to a new west-derived source (Tunik et al., 2010; Di Giulio et al., 2012, 2017; Balgord and Carrapa, 2016; Balgord, 2017; Fennell et al., 2017a, Borghi et al., 2019; Gómez et al., 2019, 2020). However, the lack of detailed sedimentological and provenance studies north of 35°S reflects the need for further studies to better understand the tectonic evolution during latest Early to Late Cretaceous times.

In the last few years, several discrepancies arose regarding the presence of a coeval volcanic arc during the Upper Cretaceous along the western margin of the Neuquén Basin (e.g., Muñoz et al., 2018; Gómez et al., 2019, 2020). Some authors speculated on a decreasing volcanic activity because of the absence of detrital zircons <100 Ma in the Neuquén Group. Moreover, an eastward arc migration is proposed in response to a shallowing of the subducted oceanic slab at ~35°S (Fennell et al., 2017a; Muñoz et al., 2018). This flat-slab stage produced an increase in the contractional deformation and the generation of a first order unconformity known as the Patagonidic (Ramos, 1988; Leanza, 2009; Tunik et al., 2010; Fennell et al., 2017b; Asurmendi et al., 2017; among others). For this paleogeographic scenario, Muñoz et al. (2018) documented differences in provenance patterns between the western and eastern Lower Cretaceous synorogenic deposits of the Neuquén Basin (~35°S). Based on this finding, Muñoz et al. (2018) suggested the presence of a topographic barrier separating the eastern and western domains, associated with the growth of the Andean fold-and-thrust belt during the Late

Cretaceous. More recently, Tapia et al. (2020) correlated this compressive stage with maximum exhumation rates estimated for the western Paleozoic basement of the Coastal Cordillera, accompanied by the development of a topographic barrier that inhibited the sediment supply derived from the contemporaneous volcanic arc to the eastern foreland basin. However, Gómez et al. (2019) found evidence of the influence of a volcanic arc during the Lower to Upper Cretaceous (Albian-Campanian) non-marine sedimentation in the foreland basin, and pyroclastic components associated with fluvial deposits were recognized within the Neuquén Group deposits (Corbella et al., 2004; Garrido, 2010; Sánchez et al., 2008, 2013; Asurmendi et al., 2017). Furthermore, Gómez et al. (2020) observed reworked tuff levels with ca. 0.60 m of thickness at 34-35°S in the Diamante Formation, which is interpreted as a direct evidence of volcanic activity during the foreland basin deposition stage. Moreover, the U-Pb detrital zircon ages as well as a petrographic analyses of the Neuquén Group and the Diamante Formation, reveal indirect evidence of the presence of an active volcanic arc after the Aptian (Tunik et al., 2010; Borghi et al., 2019; Gómez et al., 2019; among others).

The goal of this paper is to constrain the sediment provenance of the Albian to Campanian synorogenic succession in the northern Neuquén Basin and to reconstruct its evolution. With this aim, a multiproxy approach was applied with the integration of new sedimentological, petrographic and low-temperature thermochronological data with previous geochronological results obtained by Gómez et al. (2019).

2. Tectonic setting

Three different kinematic regimes have been documented in the Andes: 1) a backarc extension as a result of a slab rollback rate exceeding the ‘absolute’ velocity (normal component) of the overriding plate; 2) dominant strike-slip kinematics with a local transtension to transpression during periods of oblique convergence; and 3) a contractional deformation caused by the 'absolute' velocity (normal component) of the overriding plate exceeding the rate of the slab rollback (e.g., Schellart, 2008; Ramos, 2010; Balgord, 2016).

The well-preserved sedimentary strata of the Neuquén Basin (30°-40°S) records a complex tectonic history with spatial and temporal variations. According to Howell et al. (2005), the tectonic evolution and its sedimentary infill can be grouped into three main stages: (1) the tectonic extension phase during the Late Triassic–Early Jurassic period, manifested by isolated rift depocenters, each one showing a particular set of structural and stratigraphic features (e.g., D'Elia et al., 2020; Bechis et al., 2020; and references therein); (2) the Early Jurassic–middle Cretaceous marine and non-marine post rift basin caused by a thermal subsidence stage (Uliana and Legarreta, 1993; Legarreta and Uliana, 1996; Schwarz et al., 2016); (3) the latest Early Cretaceous to Cenozoic retro-arc foreland stage (Cobbold and Rossello, 2003; Ramos and Folguera, 2005; Mpodozis and Ramos, 2008; Tunik et al., 2010; Naipauer and Ramos, 2016; Horton, 2018). The basin was bounded by three relatively tectonically stable areas: North Patagonian Massif to the southeast and the San Rafael-Las Matras block to the north-east. To the west, the boundary was conditioned by the evolution of the Andean arc.

Important geodynamic changes occurred during the latest Mesozoic with the westward accelerated movement of the South American plate after its separation from the African plate, and the continuation of subduction processes along its western margin, with the convergence between the Nazca-Farallón and the South American plates. This setting gave rise to compressive tectonics along the western margin of the South American plate, thickening of the crust, the inversion and uplift of the Andean basins, and the continuation of the magmatic activity (Mpodozis and Ramos, 1990; Ramos and Kay, 2006; Somoza and Zaffarana, 2008; Ramos, 2009). This interpretation has been modified by several authors in the last few years suggesting that the onset of the contraction was triggered by changes in a lower mantle convection (Faccenna et al., 2017; Schellart, 2017). Chen et al. (2019) suggested that the subduction of the Farallón plate began at the northern Andes (5°S) during the Late Cretaceous period (~ 80 Ma) and propagated southwards, reaching 40°S by the early Cenozoic period (~55 Ma), based on tomographic data. More recently, Gianni et al. (2020) studied post-Gondwana synorogenic deposits and proposed that the Andean uplift was a diachronic process that propagated northward.

The study area is located in the Cordillera Principal in the central-western sector of the Mendoza Province (~34°30´S, 69°40´W) (Fig. 2a-b). The main structural features of this area are associated with the Malargüe fold-and-thrust belt (MFTB), which is characterized by large basement structures coupled with thin-skinned thrust systems developed both on top of these basement structures and along the eastern thrust front (Kozlowski et al., 1993; Manceda and Figueroa, 1995; Giambiagi et al., 2008, 2009; Turienzo, 2010; Fuentes et al., 2016).

3. Stratigraphic synthesis

The non-marine Upper Cretaceous deposits recorded south of 35°S of the Neuquén Basin are assigned to the Neuquén Group, where the sequence reaches a maximum thickness of 1,600 m (Legarreta and Gulisano, 1989; Garrido, 2010; Orts et al., 2012). There, the synorogenic deposits of the Neuquén Group are subdivided into the Río Limay, Río Neuquén and Río Colorado subgroups (Cazau and Uliana, 1973; Ramos, 1981). Cazau and Uliana (1973) pointed out that each subgroup is characterized by upward fining and thinning sequences. However, there are still many problems regarding the division and recognition of the formations. The Río Limay Subgroup represents the initial stage of the foreland basin deposition of the Neuquén Group, and it is composed by the Candeleros, Huincul and Cerro Lisandro formations. The Río Neuquén Subgroup includes the Portezuelo and Plottier formations, while the Río Colorado Subgroup is composed of the Bajo de la Carpa and the Anacleto formations. Overall, the Neuquén Group records important lateral and vertical facies changes integrating fluvial, aeolian, lacustrine, deltaic, and estuaric deposits that are controlled by allocyclic and autocyclic processes. This configuration defines diverse local depocenters that integrate the entire foreland basin (Cazau and Uliana, 1973; Leanza and Hugo, 2001; Leanza et al., 2004; Garrido, 2010; Asurmendi et al., 2017; among others). Regionally, this cyclic pattern is interrupted by the overlying Maastrichtian to Palaeocene marine facies of the lower Malargüe Group, which represents the first Atlantic-related marine succession on top of the Neuquén Group deposits (Uliana and Dellapé, 1981; Barrio, 1990; Aguirre-Urreta et al., 2008). The Neuquén Group overlies unconformably the Bajada del Agrio Group (Barremian-Albian), which was originally defined by Méndez et al. (1995) as an individual formation, and then formalized by Leanza (2003) including the Huitrín and Rayoso formations. The Huitrín Formation consists of alternating evaporitic and marginal-marine deposits with an extensive geographical occurrence in the basin that predated the final disconnection of the paleo-Pacific Ocean with the Neuquén Basin. After that, the sedimentation continued with the Rayoso Formation, which was accumulated in a shallow perennial lake of variable salinity affected by long-lived hyperpycnal flows (Leanza, 2003; Zavala et al., 2006; Lazo et al., 2017). The unconformity that separates the Bajada del Agrio Group and the Neuquén Group corresponds to a basin-scale angular unconformity named the Patagonidic unconformity (cf. Fennell et al., 2017b). This unconformity has been observed both in outcrops and in seismic data (Vergani et al., 1995; Mosquera, 2008). Nevertheless, in the study area, this angular unconformity was not recognized. For this reason, and considering the facies analysis of this work, it is assumed that the contact between the Rayoso and the Diamante formations is transitional (see the discussion section for a detailed explanation). Balgord and Carrapa (2016) proposed an erosion/non-deposition gap of 25 ma south of the study area, which includes the entire Rayoso Formation, with the Huitrín Formation directly in contact with the non-marine Late Cretaceous deposits. Similar features between both units were observed by Balgord (2016) in the Aconcagua area (32-33°S).

North of 35°S, the reddish non-marine deposits overlying the Huitrín Formation were included in the Diamante Formation initially defined by Groeber (1946). The age of detrital zircons constitutes an important tool to demonstrate a correlation between the non-marine deposits cropping out in the Mendoza Province and the Neuquén Group, but the lack of data at 34-35°S does not allow us to confirm this relationship until now. The Diamante Formation is ~300-1000 m thick in the Mendoza Province (Figs. 3-4), and records fluvial (i.e., meandering and braided systems), alluvial fan and lacustrine paleoenvironments (Cristallini and Ramos, 1996; Broens and Pereira, 2005; Balgord, 2016; Balgord and Carrapa, 2016; Mackaman-Lofland et al., 2019; Gómez et al., 2020; Lothari et al., 2020).

The absence of radiometric ages for the scarce volcanic levels interbedded in the Neuquén Group or the Diamante Formation makes it difficult to obtain an absolute age for this unit. For that reason, the age of these units are still under debate. Based on paleomagnetic studies, Dingus et al. (2000) estimated an early Campanian age for the Anacleto Formation (~83.5–79.5 Ma), while Corbella et al. (2004) obtained a zircon fission track age of 88 ± 3.9 Ma (Coniacian) for the base of the Huincul Formation of the Neuquén Group. Furthermore, several U-Pb dating on detrital zircons performed in different localities of Neuquén Group and Diamante Formation, especially south of 35°S, indicate a maximum depositional age for this units between 107 and 97 Ma (Tunik et al., 2010; Di Giulio et al., 2012, 2017; Balgord and Carrapa, 2016; Fennell et al., 2017a; Borghi et al., 2019; Gómez et al., 2019; Mackaman-Lofland et al., 2019).

In the Western Principal Cordillera of Chile, a well exposed continental Upper Cretaceous deposit named the BRCU series (Brownish Red Clastic Unit; Charrier et al., 1996) assigned to the latest Cenomanian-early Campanian by Muñoz et al. (2018), reveals sediment provenance from a coeval Cretaceous volcanic arc. According to these authors, the BRCU deposits have a chronological correlation with the Neuquén Group and the Diamante Formation in Argentina, but with differences in the provenance patterns of the U-Pb ages of their detrital zircons.

4. Multiproxy methodology

This paper contains results obtained through a combination of techniques to determine the provenance of the Albian-Campanian non-marine deposits in the northern part of the Neuquén Basin. Although several results from the application of this approach were published over the last decade, few papers include a detailed sedimentological analysis in addition to the provenance studies (e.g., Surpless and Augsburger, 2009; Di Giulio et al., 2017; Suriano et al., 2017; among others), and none of them were from this area. These analyses are the key not only to characterize the source regions, but also to understand the processes and sedimentation patterns in the foreland basins.

4.1. Stratigraphic sections, facies analysis and petrography

To carry out a detailed sedimentological analysis, two areas were logged: (1) the Arroyo Oscuro area (34°36'15.45"S; 69°44'20.00"W) and, (2) the Arroyo Las Playas area (34°33'39.42"S; 69°44'44.91"W). Both areas were integrated with studies developed in the nearby areas of Vega Grande and Vega de Los Patos (Gómez et al., 2020; Lothari et al., 2020). All these areas are located between the Atuel and the Diamante rivers (Fig. 2b-c). Thicknesses were determined using Jacob's staff. This procedure, in addition to the rock descriptions with an emphasis on lithology (including texture and composition) and on the sedimentary structures, allowed the characterization of the different sedimentary facies. Field studies enabled the recognition of the geometry of the bedsets. The Arroyo Oscuro area was the only area suitable for the analysis of the fluvial architecture, which was then correlated with the other sections. The definition of facies and their associations were used to discriminate the paleoenvironment of the Diamante Formation in the study area.

Paleocurrent measurements were performed with a Brunton® compass, and were corrected for magnetic declination in those places where exposure and outcrop-strata orientations allowed accurate measurements. These measurements provided valuable information on paleocurrents in order to shed light on the paleotopography of the area (e.g., Potter and Pettijohn, 1977; Buelow et al., 2018; Paredes et al., 2018). The imbrication of pebbles and cross-stratification were used to obtain the paleocurrent directions. Nevertheless, three-dimensional exposures were necessary to obtain true dip directions and to avoid erroneous current directions.

Measured stratigraphic areas provided the framework for a systematic collection of sandstones samples. These samples were analysed under a magnifying glass for a complete macroscopic description. Twenty-one standard 30 μm thin sections were impregnated with blue epoxy resin in order to highlight the porosity, stained with alizarin red to distinguish the dolomite and the calcite, and stained with potassium ferricyanide to distinguish the ferroan and the non-ferroan calcite following the method of Dickson (1965). After the petrographic analysis, 7 samples from the Arroyo Oscuro area and 5 samples from Arroyo Las Playas area were selected for the study of detrital modes and provenance analyses. The sandstones were classified following Folk et al. (1970) criteria, and the Gazzi-Dickinson method was used for the provenance analyses based on a 400 clast count for each thin section (Ingersoll et al., 1984). All the surveyed data was included in the discrimination provenance diagrams of Dickinson et al. (1983), along with the samples previously obtained in the Vega Grande and the Vega de Los Patos locations (Gómez et al., 2019).

4.2. Detrital zircon U-Pb geochronology

In this study, we used the U-Pb detrital zircon ages previously published by Gómez et al. (2019) from the lower part of Vega de Los Patos and the top of the Vega Grande area, with the aim of improving the multiproxy provenance analysis. These samples consisted of a medium-grained sandstone and a reworked tuff, respectively (VLP001 and VG24 samples, location in Figure 2c). U–Pb detrital zircon dating was conducted at the University of Arizona with a LA-ICP-MS equipment, following the procedures outlined in Gehrels et al. (2006, 2008). For more details about laboratory and analytical procedures see Gómez et al. (2019) and Appendix 4.

4.3. Low-temperature thermochronology: Apatite and Zircon Fission Track (AFT-ZFT)

The fission track method is based on the accumulation of narrow damage trails called “fission tracks” in uranium-rich mineral grains (e.g., apatite, zircon) and natural glasses, which form as a result of the spontaneous nuclear fission decay of ^{238}U in nature (Price and Walker, 1963; Fleischer et al., 1975). Fission tracks start to be retained in the crystal once the rock has cooled below the closure temperature (Tc) of 240 ± 20°C for ZFT and 100 ± 10°C for AFT (Laslett et al., 1987; Brandon et al., 1998; Ketcham et al., 1999), and start to reduce their length within the thermal range of 200-300°C for ZFT (ZFT partial annealing zone, PAZ; Tagami, 2005) and 60-120°C for AFT (AFT partial annealing zone, PAZ; Gleadow and Fitzgerald, 1987). When crystals are subjected to temperatures within the PAZ for a long time, the tracks are erased or annealed by thermal recovery, causing a reset of the isotopic system (Fleischer et al., 1975). Conversely, if the crystals are maintained under the PAZ, then the fission tracks are preserved.

The fission-track cooling ages were performed at La.Te. Andes S.A. laboratory (Salta, Argentina), and calculated for two samples collected from the bottom (AFT; VLP001) and the top (ZFT; 2119) of the Vegas de Los Patos stratigraphic section (Fig. 2c). The ages were obtained following the External Detector Method (EDM; Hurford and Green, 1983) and using the TrackKey software (Dunkl, 2002) (See Appendix 3 for more details about the sample preparation and the analytical procedures). The Chi squared test -P(x^2)- was applied in each case in order to evaluate overdispersed data in relation to the expectation of the statistical count for the radioactive decay process (Galbraith, 1981). For samples with P(x^2)<5%, the grain age distribution was decomposed by using the binomial peak method (Galbraith and Green, 1990) through the Binomfit software (Brandon, 2002) to identify discrete populations. A “lag time” was estimated by comparing the obtained FT cooling ages with the U-Pb detrital age of the same sample from the Diamante Formation (Gómez et al., 2019). In sedimentary rocks, this parameter represents the time a sample takes to cool below the PAZ temperatures in the source area, get transported and finally deposited (Garver et al., 1999). A rapid source cooling is evidenced by short lag times, and can be associated with a rapid source-exhumation (Reiners and Brandon, 2006; Rahl et al., 2007), or with a magmatic-source when the lag time is considerably short (Malusà et al., 2011; Malusà and Fitzgerald, 2019 and references therein).

4.4. Electron Microscope Scanning: morphological analysis of apatite and zircon grains

Apatite fission-track and U-Pb detrital zircon dating of sample VLP001 was complemented by a detailed morphological description of the apatite and zircon crystals from the same sample, through the use of an Electron Microscope Scanning (EMS). The main purpose of this approach was to distinguish populations of detrital grains with potential equivalent provenances. With this objective, 530 detrital apatite grains and 508 detrital zircon grain were randomly picked under a binocular loupe, and dispersed on a double-sided carbon tape placed on a carbon-coated aluminum stub. Each crystal was photographed with a ZEISS EVO MA15 scanning electron microscope (SEM). The morphological analysis was performed at the Instituto de Investigación en Paleobiología y Geología, Universidad Nacional de Río Negro (General Roca, Argentina). The SEM was executed in backscatter detector mode under a high vacuum with 20 kV and a working distance of ~8.5 to 5 mm, where various magnifications (~700x to 1500x) were used. The SEM was also equipped with an OXFORD X-Max 20 X-ray detector, which allowed the determination of the chemical composition of the analyses grains and verified that they were apatite crystals. The morphology of each crystal was described as rounded, subangular and angular according to the standard classification of roundness (Cox, 1927). Crystals with fractures that precluded the recognition of their morphology were not considered for the analysis.

5. Results

5.1. Sedimentological analysis

To perform the paleoenvironment interpretation from the Arroyo Oscuro and Arroyo Las Playas localities, two stratigraphic sections were measured (Figs. 3-4). These localities had not been studied in detail before and included both the Bajada del Agrio Group and the Diamante Formation deposits. Considering that there is no evidence of the Patagonidic regional unconformity along the studied sections, a transitional boundary between both units was assumed (see discussion section). Towards the top of the Arroyo

Las Playas section, the Diamante Formation shows a transitional passage to marginal marine deposits of the Saldeño Formation (Tunik, 2003, 2004).

5.1.1. Arroyo Oscuro

This section is 316 m thick (Fig. 3), where 221 m belong to the Diamante Formation while 70 m and 25 m belong to the Huitrín and Rayoso formations, respectively. Three main textural groups of sedimentary facies were identified: (1) conglomeratic and (2) sandy clastic facies, (3) calcareous and evaporitic facies. A total of nine sedimentary facies have been characterized (Table A1.1, Appendix 1). Furthermore, we classified these deposits into three main facies associations; A: restricted brackish lake, B: sheet-flood deposit, C: channelized fluvial deposits.

Conglomeratic facies (Table A1.1., Gmm, Gcm, Gct) are the least abundant in the area and show fining-upward co-sets with variable thicknesses (up to 3 m) and lateral extensions (from 1 to 27 m). The geometry of the sedimentary bodies is variable, with a predominance of lenticular and chaotic forms. Cut and fill structures have been observed in these facies. The presence of isolated angular clasts of variable sizes (~6 cm) is common. This feature was frequently observed in the non-channelized fluvial deposits of both sections. The most common arrangement begins with coarse to fine conglomeratic (Gmm, Gcm, Gct), followed by coarse-sandstone facies and finishes with medium to fine sandstone facies (St, Sh, Sl) with bioturbation (Sm). A massive character predominates in the sedimentary deposits, and the presence of 3D channelized sedimentary bodies and imbricated clast is restricted; however, they allowed the measurements of paleocurrent data (Fig. 3). Another important feature recognized is the difference in the composition of the conglomerates along the entire section. While the lower part of the section shows a predominance of acid volcanic clasts (especially rhyolites), the middle and the upper part are composed almost exclusively by clasts of limestone.

The sandy facies are predominant, with even more varied sedimentary structures than the previously mentioned facies. Four facies have been recognized: St, Sh, Sm, and Sl (Table A1.1, Appendix 1). Together, they represent a continuous succession of channels and bars that are linked laterally and vertically, exhibiting both ribbon and sheet geometries as well as individual bodies. Bioturbation is very common and frequent, obliterating the primary structure. In the same way, an increase in bioturbation towards the middle and upper part of the section has been observed. Regarding the ichnological content, *Scoyenia* isp., *Skolithos* isp., and *Arenicolites* isp. were recognized. Furthermore, undifferentiated vertical and horizontal tubes have been identified. Additionally, the presence of mottled massive sandstones with carbonate nodules is very common.

5.1.2. Arroyo Las Playas

A detailed examination of the succession in the Arroyo Las Playas area with a total thickness of 614 m, allowed the identification of 532 m belonging to the Diamante Formation, while 70 m and 12 m belong to the Huitrín and Rayoso formations, respectively. The essential characteristics of these facies are summarized in Table A1.1 (Appendix 1). Thirteen sedimentary facies were distinguished and divided into four textural groups; (1) conglomeratic, (2) sandy and (3) mudstones clastic facies, and (4) calcareous and evaporitic facies. As the result of the facies analysis, five facies associations were defined and interpreted; A: restricted brackish lake, B: ephemeral lake, C: sheet-flood, D: channel and bars and E: floodplain.

In this area, as well as in the other sections, the conglomeratic facies were comprised into sedimentary bodies with an erosive base and fining-upward trends. Internally, these bodies correspond to a clast-supported conglomerate with parallel stratification (Ghc). Clasts are angular to subangular, composed by volcanic lithics and reach up to 3-4 cm on the A-Axis. A massive matrix-supported conglomerate (Gmm) with subangular to subrounded clasts of 6 cm long (along the A-axis), and a massive clast-supported conglomerate (Gcm) with volcanic and limestone clasts of up to 7 cm long (towards the top of the section) have been also identified (Fig. 5a). Finally, clast-supported conglomerate facies with tangential and festoon cross-bedding (Gct) were identified, consisting mainly of angular to subrounded volcanic clasts, mainly of rhyolitic composition, although clasts of dacite, trachyte, and andesite were also observed. Those volcanic clasts present themselves in various ranges of sizes (1-7 cm). Conglomerates composed almost exclusively of limestone clasts can also be observed at the top of the section, as well as subangular red-siltstone clasts.

Regarding sandy facies, medium to very fine sandstone with parallel stratification (Sh) have been identified, which eventually showed internal structures of parallel and ripple cross laminations, as well as some pedogenetic features such as mottling. Sandstone with parallel lamination (Sl), medium to fine-grained pebbly sandstone (SGm) with isolated clasts, and medium to very fine massive sandstone (Sm), which correspond to the most abundant sandstone within the surveyed area, have also been recognized (Fig. 5b).

The fine-grained facies are represented by massive mudstones (Fm), normally semi-covered, mudstones with parallel lamination (Fl), and mudstones with parallel bedding (Fh). These facies normally show pedogenetic features such as mottled, slickensides, blocky and subangular peds, and undifferentiated bioturbations.

The calcareous and evaporitic facies are present in the basal part of the succession of the Arroyo Las Playas area as well as the Arroyo Oscuro area (Figs. 3-4) and consists of 70 m-thick gypsum/massive anhydrite beds (Em) and less common gypsum/laminate anhydrite, which are interbedded with stratified limestone (Lh).

5.1.3. Paleocurrent analysis

A total of 44 paleocurrent directions were measured in the Arroyo Oscuro area, evidencing a significant change between the bottom and the top of the section (Fig. 3), revealing an important shift in the paleocurrent direction. They are east-derived (on average towards 285° Az) at the bottom and west-derived (on average towards 093° Az) at the top. In contrast, in the Arroyo Las Playas area, the paleocurrent data is limited to just one (towards 15° Az) at the top, due to the absence of 3D measurable sedimentary structures and the scarce levels with imbricated clasts.

5.2. Petrographic description and modal analysis

For the purpose of this study, we include new petrography data from the Albian to Campanian deposits of the Arroyo Oscuro and the Arroyo Las Playas localities. They are compared with the data obtained from nearby study areas (Gómez et al., 2020; Lothari et al., 2020). Petrographic observations facilitated a general description of the principal components from the clastic fraction. Different types of quartz (Q), feldspars (F), and lithic fragments (L) were discriminated and quantified. Likewise, the features of the cements and the presence of heavy minerals in the thin sections were observed. The sandstones were classified following the proposal of Folk et al. (1970) and were mainly lithic feldarenite and feldespathic litharenite. The average value of the percentage in weight for these samples is $Q_{50}F_{24}L_{25}$ (Appendix 1-Fig. 7a). Quartz was the predominant component in all the samples (50%) and appears in the form of monocrystalline (33%) and polycrystalline in subordinate proportions (7.2%). The most abundant type of quartz is monocrystalline with straight extinction (26.4%), it generally appears well rounded, and in some cases with inclusions. Quartz, as a fragment of a volcanic rock (0.9%) was also recognized, as well as quartz with an undulatory extinction (5.7%). In particular, almost all samples contain embayment quartz (Fig. 6c). The variation in the quartz content within the two areas shows a decrease in the middle part of both sections. Feldspars constitute approximately 21-33% of the samples. Alkaline feldspar is the most common type and was identified by Carlsbad or tartan twinning, when present. Plagioclase feldspar was identified primarily by albite twinning. Both types of feldspars normally show sericitic and argillic alteration, but it is more frequent in alkaline feldspar. Alkaline feldspar and plagioclase were recognized as volcanic rock crystals in subordinate amounts. Furthermore, there was no correlation between either profile, or from the base to the top. In the Arroyo Oscuro area, the plagioclase/total feldspar ratio does not vary and its value remains at 0.35, while in the Arroyo Las Playas area, there is a high value at the bottom section, with a ratio of 0.65 and the ratio remains at 0.45 on average. Recognition of different categories of lithic fragments is very important in provenance studies. Lithic fragments reach on average 25% of the clastic fraction and are almost exclusively volcanic, and more specifically the paleovolcanic type following the criteria used by Critelli and Ingersoll (1995). Paleovolcanic lithic fragments with granular (3%) and seriate (5%) textures are predominant, although volcanic fragments with lathwork (0.6%), microlitic (0.2%) and pyroclastic (1%) with eutaxitic textures were also observed (Fig. 6a). It is very important to note the presence of calcareous lithic fragments in the mid and top part of the Arroyo Oscuro section, although they were in low proportions (on average 1%) (Fig. 6d). In contrast, altered lithic fragments were observed in relatively high proportions (on average 6%). Finally, sedimentary lithic grains, metamorphic rock fragments and plutonic lithic clasts were observed, as well, in very low proportions (less than 2%). Regarding the types of cement, ferruginous is the most common (5.9%), followed by calcareous (4.2%) argillaceous (2%), and zeolitic (1.7%) types. The cement appears as pore filling, pore lining and, more scarcely, as poikilotopic. The zeolitic cement corresponds to analcime type, which occurs as pore filling and in subhedral crystals related to calcite cementation. The presence of this type of cement is important for the provenance interpretation (see discussion below). Minor components correspond to micas and opaques, along with heavy minerals such as zircons and apatite among others (Fig. 6e-f).

Regarding sandstone point counting, a recalculated modal composition was carried out (Appendix 1) and plotted on a tectonic discrimination diagram of Dickinson et al. (1983). The Qt-F-Li graph indicates that the analysed samples from both sections correspond to recycled orogen. Furthermore, in the Qm-F-Lt diagram, the distributions of the samples are clustered in mixed and dissected arc fields. Figure 7b shows both graphs, as well as previous data obtained from other sections in the study area (Gómez et al., 2019).

5.3. Apatite and zircon fission track

The VLP001 sample from the lower part of the Diamante Formation reported an Early Cretaceous (Albian) AFT central cooling age of 111.9 ± 13.6 Ma (Table 1), linked to a unique statistical population of grain-ages with a low degree of dispersion and a $P(x^2)>5\%$ value (Fig. 8-Ia). The probability density distribution of the grain-ages indicates a major peak between 100 and 120 Ma, followed by a subordinated peak at ~200 Ma (Fig. 8-Ic); both correlative with those evidenced in the cumulative grain-age distribution plot (Fig. 8-Ib).

Thirty-seven zircon crystals from the Diamante Formation (sample 2119) dated by ZFT, did not pass the chi square test ($P(x^2)<<5\%$, Fig. 8-IIa), resulting in two discrete populations of grain-ages of P_1 = 161 ± 16.4 Ma (71%) and P_2 = 265.2± 46.5 Ma (29%) (Table 1, Fig. 8-IIa). Both populations are visible in the probability density distribution and the cumulative grain-age distribution plots (Figs. 8-IIb-c). See Appendix 3 for more details.

5.4. Morphological analysis of apatite and zircon crystals

From the total number of analysed apatite crystals (n=530) of the VLP001 sample (Fig. 9), the morphological analysis of 383 apatites, showed a predominance of rounded crystals (Fig. 9c), corresponding to 56% of the total. Angular (Fig. 9a) and subangular (Fig. 9b) crystals accounted for proportions of 21% and 23%, respectively, while 147 apatite grains with fractures were not considered for this analysis (See Appendix 5 for details).

In the case of the zircon crystals from the VLP001 sample, from the total number of analysed grains (n=508) (Fig. 10), the morphological analysis of 361 zircons sample showed a predominance of subangular crystals (Fig. 10b), corresponding to 40% of the total. Angular (Fig. 10a) and rounded (Fig. 10c) crystals accounted for proportions of 33% and 27%, respectively, while 147 zircon grains with fractures were not considered for this analysis (See Appendix 6 for further details).

6. Discussion

6.1. Paleoenvironmental interpretation

The facies associations previously defined for the Arroyo Oscuro and the Arroyo Las Playas areas indicate particular depositional environments.

In the case of the Huitrín and the Rayoso formations (Bajada del Agrio Group), the facies associations represent a restricted marginal marine system that evolved to an ephemeral lacustrine environment. The Huitrín Formation is linked to an inland hypersaline shallow sea with high temperatures resulting in high evaporation rates, as well as periodic siliciclastic depositional stages. The presence of fine-grained siliciclastic facies at the top of the succession could suggest meteoric sediments coming from emerged areas or/and changes at the base level (Roulston and Waugh, 1983). The connection with the proto-Pacific Ocean located to the west was limited by a magmatic arc, which was a topographic barrier that partially restricted the influx of seawater. This sedimentary sequence depicts the transition between the backarc and the foreland stages during the Early to the Late Cretaceous periods (Veiga and Vergani, 2011; Gabriele, 2016; Lothari et al., 2020; among others).

The Arroyo Oscuro and the Arroyo Las Playas areas, as well as previously studied sections of Vega Grande and Vega de los Patos (Gómez et al., 2020; Lothari et al., 2020), reveal that the Diamante Formation comprises a complex fluvial system that reflects changes in depositional controls (e.g., tectonic and climate), and in the accommodation and sediment supply conditions represented by shifts in the floodplain deposit's thickness and the stacking of channels (Table A1.1, Appendix 1). Furthermore, the changes of the paleo-slope resulted in a variation in the facies associations and the geometry of the sedimentary bodies (Schumm, 1981; Ramon and Croos, 2002; Bridge, 2003; Miall, 2014). Based on these characteristics, we propose that the Diamante Formation was deposited by a braided fluvial system that evolved over time to a meandering fluvial system. Furthermore, we argue that the Diamante Formation would have been part of the medial zone of a fluvial fan or Distributive Fluvial System (DFS) (Nichols and Fisher, 2007; North and Warwick, 2007; Cain and Mountney, 2009; Hartley et al., 2010; Weissmann et al., 2010; Miall, 2014).

The coarse-grained facies (Gmm, Gcm, Gct, Sgm, St, Sh) of the Arroyo Oscuro and the Arroyo Las Playas areas show distinctive processes associated with braided and meandering fluvial systems, with the stacking of channels and bars limited by erosive surfaces, and the presence of cut and fill structures that represent the overlapping of various events, leading to multi-story channel. The presence of juxtaposed younger and older individual channels lumped together into a composite body is very common, and is associated with successive relocations of the river (avulsion). The ratios between the width and the thickness of fluvial-channel bodies is an average of 0.5 to 9, which is evidence of narrow to broad ribbons based on the classification of Gibling (2006) (Fig. 5b). Considering the geomorphic setting, the geometry, and the internal characteristics of these fluvial-channel bodies, they can be collectively defined as parts of distributive systems (Gibling, 2006). A multiepisodic sandy-gravel channelized complex is recognized within the facies association C in the middle part of the Arroyo Oscuro area (Fig. 5c-d), based on the methodology suggested by Miall (1985, 1996) and Cain and Mountney (2009 and references therein). This architectural element describes a simple lateral and vertical arrangement of sedimentary facies of clast-supported conglomerates with tangential and festoon cross-beddings (Gct), medium to fine sandstones with planar parallel stratifications (Sh), and fine to very fine massive sandstones with bioturbations (Sm). This setting conforms to packages of amalgamated macro-channels of a 2 to 6 m thickness, interbedded with non-channelized sandy facies (Fig. 5e-f).

There is a predominance of massive structures, both in non-channelized conglomerates and sandy facies (Gmm, Gcm, Sgm, Sm), probably associated with flooding events responsible for debris flow deposits. These deposits describe irregular and sharp – often non-erosional – bases, and form lobes, ribbons or sheets (e.g., Miall, 1985, 1996; Bridge, 2003). The presence of isolated clasts within these deposits is interpreted as traction-carpets deposited by a high-density gravel turbidity current (Lowe, 1982; Mutti, 1992). Furthermore, it cannot be ruled out that the massive character of these facies could be related to the destruction of primary depositional structures by bioturbation.

Fine-grained facies (Fm, Fl, Fh), are part of floodplain facies associations and show vertical accretion deposits with a maximum thickness of ~80 m. The main processes associated with these sedimentary facies are the decanting of the fine material produced during the final stage of the decelerated flows. The high level of bioturbation in these facies and the presence of mottled, slickensides, blocky and subangular peds, are evidence of pedogenetic processes. The high percentage of floodplain facies associations in the study area, as well as in nearby localities (Gómez et al., 2020; Lothari et al., 2020), could be related to a combination of tectonic and climate factors during sedimentation processes. In the studied sections, these deposits are frequently truncated by isolated channel-bodies with ~2 m of thickness. The presence of these isolated deposits would be explained by a typical mechanism of deposition called "incisional avulsion" (Slingerland and Smith, 2004).

6.2. Provenance analysis: Clasts composition and paleocurrent data

Acid and intermediate volcanic (rhyolites-trachytes) clasts are the most common rock constituents in the studied succession. These fragments could be associated with the Choiyoi Group (Permian-Triassic), which integrates the structural basement of the Neuquén Basin, and are very common in other sections of the Neuquén Group from different sectors of the basin (Garrido et al., 2010; Balgord and Carrapa et al., 2016; Borghi et al., 2019; among others). These clasts could derive from the erosion of the eastern San Rafael Block, if we consider this area as a positive forebulge as Balgord and Carrapa (2016) proposed. A minor number of andesitic-dacitic volcanic clasts was also recognized in the Arroyo Oscuro and the Arroyo Las Playas areas probably associated with the Choiyoi Group. More recently, Martos et al. (2020) described the presence of metamorphic clasts and measured north-derived paleocurrents in Vega de Los Patos area, which would indicate that the Frontal Cordillera could have been a potential source.

Red-siltstones are present as subangular clasts in conglomerate facies at the top of Arroyo Las Playas section and can be associated with the erosion and redeposition of the underlying Rayoso or Tordillo formations. Of particular relevance for the provenance analysis is the occurrence of limestone lithic clasts starting from the middle part of both sections and persisting to the top of the sequence. This macroscopic observation was also recognized in neighbouring study areas (Gómez et al., 2019; Lothari et al., 2020). Moreover, limestone lithic clasts within the Diamante Formation are evident to the west (Broens and Pereira, 2005). The regional occurrence of these calcareous clasts (Tunik, 2001; Balgord and Carrapa, 2016; Fennell et al., 2017a; Gómez et al., 2019; Borghi et al., 2019; Lothari et al., 2020), would suggest the presence of a common regional source associated with the exhumation of the Andean orogen west of the study area, and the erosion of the Mendoza Group (Upper Jurassic-Lower Cretaceous) or the Lotena Group (Middle-Upper Jurassic), representing a regional depositional event.

Paleocurrent measurements from the Arroyo Oscuro area (n=44; Fig. 3) evidence an important change of direction in the middle part of the section. The orientation of imbricated clasts and 3D measurable sedimentary structures describes a W-directed paleoflow for the first part of the section (average = 285°Az; n=35), followed by an E-directed paleoflow in the upper part (average = 093°Az; n=9), possibly derived from the San Rafael Block located to the east, and the Andean orogen situated to the west, respectively (see the U-Pb detrital zircons peaks to compare, Fig. 8-III). Even though the role and exhumation of the San Rafael Block during Mesozoic times remains unclear, the presence of a positive topography eastwards becomes evident. This interpretation is consistent with the hypothesis of a forebulge or peripheral bulge area associated with the Andean fold-and-thrust belt foreland (Tunik et al., 2010; Di Giulio et al., 2012; Borghi et al., 2019). In fact, if we consider the proximity (~50 km) between the non-marine deposits of the Diamante Formation in the study area and the San Rafael Block, we can infer that the variations in the provenance patterns are part of a coalescent fluvial system with a predominance of W-directed paleocurrents during the initial deposition of the Diamante

Formation deposits. Then, a shift in the paleocurrent direction occurred, provoked by the onset of the Andean orogeny (Fig. 11).

6.3. Onset of foreland basin deposition: diachronism or synchronism?

The analysis of the U-Pb maximum depositional ages documented for non-marine Lower to Upper Cretaceous synorogenic deposits throughout the Neuquén Basin in the last decade, integrated with those obtained from the base of the Diamante and the Candeleros formations, should permit us to better constrain the beginning of the foreland basin infill (Fig. 12). Nevertheless, differences exist when comparing all maximum depositional ages proposed by each author from different sectors of the basin. The Candeleros Formation yields a maximum depositional age of 100.5 ± 2.1 **(n=1)** and 104.3 ± 2.5 Ma **(n=1)** (Tunik et al., 2010); and Di Giulio et al. (2012) obtained similar ages of 102 ± 2 Ma **(n=5)** and 100 ± 8 Ma **(n=1)**, both for the Agrio fold-and-thrust belt (37°-38°S). In the southern Mendoza province (35°-36°S), Fennell et al. (2017a) obtained a 100.2 ± 2.1 Ma age **(n=1)** and Balgord and Carrapa (2016) a 97 ± 2 Ma age **(n=4)** for the base of the Río Limay-Subgroup and the Diamante Formation, respectively. Recently, at the same latitudes, Borghi et al. (2019) defined two maximum depositional ages for the Río Limay-Subgroup, one of 101.6 ± 2.6 Ma **(n=2)** near the contact with the Rayoso Formation, and another of 91.4 ± 2.3 Ma **(n=4)** 70 m above the first age obtained. Our previous studies in a nearby locality yielded two maximum depositional ages of 107.2 ± 1.4 Ma **(n=4)** for a litharenite deposit from the lower part of the Vega de Los Patos area (Fig. 8-III), and 91.1 ± 2.2 Ma **(n=3)** for a reworked-tuff from the top of Vega Grande section (Gómez et al., 2019).

The lack of a tight correlation between the maximum depositional ages for the first Andean synorogenic deposits, likely relates to the method applied for the estimation of the ages in each case, rather than a diachronic deposition. The methods applied for that purpose range from the most robust (e.g., two or more young grain-ages that overlap) to the least robust (e.g., the -unique- youngest grain-age) (Dickinson and Gehrels, 2009), sometimes involving a certain grade of subjectivity. This becomes evident when a detailed comparison between the distributions of the youngest grain-ages of each sample is performed. If all youngest U-Pb detrital zircons from previous studies (Tunik et al., 2010; Di Giulio et al., 2012; Balgord and Carrapa, 2016; Fennell et al., 2017a, Borghi et al., 2019; Gómez et al., 2019) are analysed in detail, a common group of overlapped grain-ages which cluster around ~109-107 Ma (Fig. 12) can be recognized for each sample. Considering that the number of zircons involved in this interval of ages is statistically more robust than selecting a unique age in each case (Tucker et al., 2013; Coutts et al., 2019; Vermeesch, 2021), we argue for an Albian age (Lower Cretaceous) for the Candeleros Formation (or for the base of the Diamante Formation).

6.4. Lower Cretaceous to Upper Cretaceous volcanic activity

The application of a multiproxy approach for the provenance analysis of the Arroyo Oscuro and the Arroyo Las Playas areas, and its integration with pre-existing data (Gómez et al., 2019; Lothari et al., 2020), allowed us to identify a potential signal of volcanic activity at 34-35° for the Albian. The petrographic analysis developed in the Arroyo Oscuro and the Arroyo Las Playas areas evidence an important presence of volcanic lithic fragments, where felsitic and granular textures are common (Figs. 6-7). The same analysis from the Vega Grande area also showed subordinated vitric textures (Gómez et al., 2019). These characteristics could be indicative of a potential volcanic source related to an incipient Late Jurassic-Early Cretaceous magmatic arc located to the west, as already proposed by Vergara et al. (1995). According to Affolter and Ingersoll (2019), the granular textures are usually related to high-SiO_2 sources. These authors also explain the importance of considering the preservation of textural and compositional types. Vitric textures are the most reactive because the glass is fragile, especially in the form of glass shards and bubble walls. Conversely, lithic fragments with high-SiO_2 content are generally more stable during weathering. This could explain the lack of vitric textures in the petrographic thin sections of the Arroyo Oscuro and the Arroyo Las Playas areas. Furthermore, pyroclastic lithic fragments with eutaxitic textures, embayment on the quartz, and analcime as cement, have also been observed. The analcime is very common in volcanic environments since it could be formed by dissolution and precipitation from the volcanic glass. Sandstone samples show medium to low plagioclase/total K-feldspar ratios, ranging from 0.65 to 0.45 (from the base to the top of the Arroyo Las Playas area). This trend could indicate a felsic plutonic provenance (e.g., Critelli and Ingersoll, 1995; Critelli and Nilsen, 2000).

AFT analysis of VLP001 reveals a unique central cooling age of 111.9 ± 13.6 Ma (Albian) ($P(x^2) > 5$, Fig. 8a). This age could reflect diverse hypothetical scenarios: (1) Albian cooling/exhumation in situ, with an erased inherited signal by a total reset after deposition; (2) cooling/exhumation of the source during Albian times; or (3) magmatic cooling of a volcanic source during Albian times. Considering that the maximum thickness of the sediments registered since Albian times in the study area are in the range of ~1,165-1,373 m (Turienzo et al., 2012), a total reset of the AFT isotopic system of the VLP001 sample after deposition is not feasible. The estimation of a lag time between both the AFT and the U-Pb maximum depositional age of the VLP001 sample (111.9 ± 13.6 Ma and 107.2 ± 1.4 Ma, respectively) results in ca. 3 ma, with both ages overlapped, considering their range of analytical uncertainty. This time lapse is considerably tight to account for the exhumation of the source, erosion, transport and deposition, being better explained by a rapid magmatic cooling of the source (e.g., Malusà et al., 2011; Malusà and Fitzgerald, 2019 and references therein).

It is important to highlight that most of the apatite crystals of the VLP001 sample that were analysed by AFT, have euhedral to subhedral morphologies. Rounded (anhedral) apatite-crystals were not included for measuring purposes because of the problems of finding crystals with an appropriate orientation (Dpar parallel to the c-crystallographic axis). Therefore, we infer that the central cooling age obtained represents the same population of apatites derived from a volcanic source, as suggested by the estimated short lag time.

The morphological analysis of 530 apatite and 508 zircon crystals from the VLP001 sample through SEM, reveals the presence of three populations of grains: rounded (56%), subangular (23%), and angular (21%) (Fig. 9) for the apatites analysis, and subangular (40%), angular (33%) and rounded (27%) (Fig. 10) for the zircons analysis. This approach was applied to observe morphological features of these grains and used as a fingerprint of the provenance source in the foreland basin deposits (e.g., Fedo et al., 2003; Finzel, 2017). The high proportion of angular and subangular apatites and zircons is in good agreement with a volcanic provenance whereas the prevalence of rounded grains in the sample could evidence the recycling of the Mesozoic sedimentary units.

Based on the petrological and sedimentological analysis, and its integration with AFT and U-Pb ages of the VLP001 sample, we argue for the presence of a volcanic arc located west of the study area, coeval with a non-marine Diamante Formation deposition during the latest Early Cretaceous times (119-102 Ma). The volcanic activity towards the Late Cretaceous becomes evident given the recognition of the reworked-tuff interbedded in the Vega Grande area where one of these layers yielded a maximum depositional age of 91.1 ± 2.2 Ma (Gómez et al., 2019). The youngest detrital zircons of this sample (~92-80 Ma), is also correlative with the U-Pb detrital zircon-ages provided for the Mesozoic units from the western Andean slope, which are contemporaneous with the deposition of the Diamante Formation (Muñoz et al., 2018).

Our proposal matches the existence of a continuous activity of a magmatic arc suggested for the Late Jurassic-Late Cretaceous period and the Lower Cretaceous contractional episode, both suggested for the western slope of the Andes at these latitudes (Charrier et al., 2007; Oliveros et al., 2018; Tapia et al., 2020) (Fig. 11). Additionally, Balgord (2017) observed continuous volcanism from 190 to 140 Ma, followed by major age populations at 129 Ma, 110 Ma, 67 Ma, 52 Ma, 16 Ma, and 7 Ma, based on a combination of a large bulk of detrital zircon data from the Neuquén basin between 34° and 40°S. This author proposed a lull in volcanic activity during the retroarc foreland basin deposition, with a hiatus of 40 ma between 110 Ma and the first high-flux event after the initial shortening at 70 Ma.

Mesozoic units from the Chilean slope of the Andes (33-36°S) evidence a synorogenic nature; as well as a volcanic provenance represented by volcanoclastic and volcanic deposits of the BRCU, Las Chilcas, and the Colimapu formations (Boyce et al., 2014; Muñoz et al., 2018; Tapia et al., 2020). The U-Pb zircon-ages indicate an Albian depositional age for the Las Chilcas Formation in the forearc (Godoy et al., 2009; Boyce et al., 2020; Contreras and Schilling, *in press*), coincident with the maximum depositional age of 107.2 ± 1.4 Ma obtained from the Vega de Los Patos area located in the retroarc foreland basin (Gómez et al., 2019). However, Tapia et al. (2020) proposed that the compressive deformation along the Coastal Cordillera at ~35° S would have begun at 113 Ma with the deposition of the Las Chilcas Formation along the eastern slope of the late Early Cretaceous orogen, in agreement with an accelerated exhumation period registered between 113 and 80 Ma along the Paleozoic metamorphic basement of the same region (Willner et al., 2005). Moreover, the maximum depositional age of 107.2 ± 1.4 Ma matches the onset of the Andean exhumation and denudation proposed by Galetto et al. (2021) for the Albian (~110 Ma), based on inverse thermo-numerical modeling of multiple thermochronometers from the northern Chos Malal fold-and-thrust belt (36-37°S). At an intercontinental scale, this proposal coincides with a remarkable increase in plate spreading rates, interpreted as the responsible for the consequent Andean compressional stage (Somoza and Zaffarana, 2008; Matthews et al., 2012; Müller et al., 2016).

6.5. Significance of Permian and Late Jurassic zircon-ages

A ZFT analysis of the top of the Diamante Formation in the Vega de Los Patos area (2119 sample), yielded two discrete populations of grain-ages of P_1 = 161.1 ± 16.4 Ma and P_2 = 265.2 ± 46.5 Ma (Table 1, Fig. 8). These results reveal a non-reseted ZFT isotopic system, where both ages reflect source-cooling. This is in agreement with the maximum thickness of the sedimentary sequence registered since Albian times in the study area (~1165-1373 m, Turienzo et al., 2012), not enough to reset/partial reset the ZFT isotopic system of the 2119 sample. Both populations are consistent and overlapped (considering the range of analytical uncertainty) with the second and third peaks visible on the frequency histogram and the relative probability plot of the U-Pb detrital ages from the VLP001 sample (148 and 267 Ma, respectively; Fig. 8). In this sense, both the Upper Jurassic U-Pb and the ZFT zircons-ages (U-Pb = ~148 Ma, ZFT P_1 = 161.1 ± 16.35 Ma) could derive from the Jurassic volcanic arc situated in the Coastal Cordillera by that time (Oliveros et al., 2006; Tapia et al., 2020), as well as from the erosion and recycling of the Mesozoic units (Rossel et al., 2014; Naipauer and Ramos, 2016; Naipauer et al., 2018). The Permian U-Pb and the ZFT zircon-ages (U-Pb = ~267 Ma, ZFT P_2 = 265.2 ± 46.5 Ma) could derive from the reworked pre-Mesozoic units of the Choiyoi Group (Sato et al., 2015) (Fig. 11). Regarding the absence of the cretaceous cooling age-population in this sample, it could indicate a decrease in the volcanic input to the top of the Vega de Los Patos section.

7. Conclusions

A multiproxy provenance analysis developed on the Arroyo Oscuro and the Arroyo Las Playas areas, and its combination with previous studies, evidence the presence of coeval volcanic activity during the onset of the Andean foreland basin at 34-35°S. The evidence that support our proposal are summarized below, integrated with paleoenvironment and regional tectonic scenarios:

- The stratigraphic sequence of the study area records the transition between the backarc and the foreland basin stages in the Neuquén Basin. Both stages are represented by a transitional boundary between the Bajada del Agrio Group and the Diamante Formation. The Rayoso and the Huitrín formations (Bajada del Agrio Group) correspond to a restricted marginal marine system, evolving over time towards an ephemeral lake environment. The analysis of the non-marine deposits of the Diamante Formation allow the identification of a braided fluvial system that evolves towards a meandering fluvial system, as part of the medial zone of a fluvial fan or Distributive Fluvial System (DFS). Our results evidence that the Diamante Formation was deposited in a foredeep depozone with sediments derived both from the Andean fold-and-thrust belt, and the magmatic arc located to the west, as well as from the forebulge located to the east.

- There is a predominance of volcanic clasts with acid to intermediate compositions through the Arroyo Oscuro and the Arroyo Las Playas sections, with a particular occurrence of calcareous clasts in their middle parts. This change was accompanied by a shift in the paleocurrent direction (more evident in the Arroyo Oscuro area) that reveal a mixed provenance from the western and the eastern areas (Andean Range and basement forebulge, respectively) for the first foreland deposits, as well as a notable increase in the western input for the second half of the sections. Additionally, petrographic analyses show a predominance of feldspathic litharenite according to the Folk et al. (1970) classification, while the source areas are mainly recycled orogen (diagram QFL) and mixed and dissected arc (diagram QmFLt), according to Dickinson et al. (1983).

- The analysis of the U-Pb maximum depositional ages documented for non-marine Upper Cretaceous deposits throughout the Neuquén Basin, integrated with those obtained from the bottom of the Diamante and the Candeleros formations, evidence a persistent group of overlapped grain-ages that cluster around ~109-107 Ma. Based on this correlation, and on the pursuit of reviewing the methods applied for the statistical analysis of the U-Pb detrital zircon-ages, we propose an Albian age for the base of the Diamante Formation and the Candeleros Formation, and we argue for a re-evaluation of the diachronism between the first foreland deposits of the Neuquén Basin.

- Apatite fission track analyses from the bottom of the Diamante Formation (VLP001) yield an Albian central cooling age, derived from the measurement of euhedral to subhedral apatite crystals. The comparison between the AFT central age and the U-Pb maximum depositional age of the same sample allows the estimation of a short lag time of ca. 3 ma, interpreted as evidence of a volcanic arc provenance during Albian times. In this scenario, the AFT central age would represent the rapid cooling of a magmatic source. Additionally, morphological analysis of apatite and zircon crystals from VLP001 through SEM images, reveal a notable presence of angular (euhedral) crystals, likely derived from a magmatic source, with subordinated rounded crystals that reflect a sedimentary input as well.

- Zircon fission track analyses of sample 2119 collected from the top of the Diamante Formation yield two discrete populations of grain-ages of ca. 161.1 Ma and ca. 265.2 Ma. Both are interpreted as inherited signals, in reflection of source-cooling. The first population of apatites could derive from the erosion of the Upper Jurassic magmatic arc, therefore revealing its magmatic cooling. The second population could derive from the erosion of the Choiyoi Group units, reflecting their magmatic cooling during Permian times.

- The results presented in this work suggest a coeval volcanic activity during the Diamante Formation deposition, and are consistent with the volcanic and volcaniclastic processes documented in the Chilean Mesozoic sediments west of the study area. The new data provided in this work highlight that deeper studies are needed to better constraint the onset of the foreland basin at these latitudes, and to better define the role of the volcanic arc and its influence on the foreland deposits in the Southern Andes during the latest Early-Late Cretaceous period.

Acknowledgments

This work is based on research within R. Gómez’s Ph.D. project and supported by CONICET (PUE 0031CO), and subsidies from the Universidad Nacional de Río Negro and the Agencia de Promoción Científica y Tecnológica (UNRN-40A-321, ANPCyT PICT 2018-00917, and PICT-2017-3259). The authors would like to acknowledge the Laboratorio de Termocronología La.Te. Andes S.A. (Salta, Argentina), and Sofía Bordese for their collaboration with the low-temperature thermochronology analyses. We are grateful for the important collaboration of Juan Ignacio Ison with the preparation of the thin sections and Mavi Buhler with the improvement of the English of this manuscript. The authors would especially like to thank Dr. Maximiliano Naipauer, Dr. Lucas Fennell and the editor-in-Chief Dr. Eduardo Koutsoukos for their constructive review that helped to refine and clarify this manuscript.

References

Affolter, M.D., Ingersoll, R.V., 2019. Quantitative Analysis of Volcanic Lithic Fragments. Journal of Sedimentary Research 89 (6), 479–486. doi: https://doi.org/10.2110/jsr.2019.30.

Aguirre-Urreta, M.B., Pazos, P.J., Lazo, D.G., Fanning, C.M., Litvak, V.D., 2008. First U–Pb SHRIMP age of the Hauterivian stage, Neuquén Basin, Argentina. Journal of South American Earth Science 26, 91–99.

Asurmendi, E., Sánchez, M.L., Fennell, L., 2017. Neuquén Group (Upper Cretaceous): a case of underfilled-overfilled cycles in an Andean foreland basin, Neuquen basin, Argentina. Journal of South American Earth Science 80, 444–459.

Balgord, E.A., 2016. Triassic to Neogene Evolution of the Andean Retroarc: Neuquén Basin, Argentina. Ph.D. thesis. The University of Arizona. Online version at: https://repository.arizona.edu/handle/10150/595810

Balgord, E., 2017. Triassic to Neogene evolution of the south-central Andean arc determined by detrital zircon U-Pb and Hf analysis of Neuquén Basin strata, central Argentina (34°S–40°S). Lithosphere 9, 453–462.

Balgord, E.A., Carrapa, B., 2016. Basin evolution of upper cretaceous–lower cenozoic strata in the Malargüe fold-and-thrust belt: northern Neuquén Basin, Argentina. Basin Research 28 (2), 183–206.

Barrio, C.A., 1990. Late cretaceous early tertiary sedimentation in a semi-arid foreland basin (Neuquén Basin, western Argentina). Sedimentary Geology (66), 255-275.

Bechis, F., Giambiagi, L.B., Tunik, M.A., Suriano, J., Lanés, S., Mescua, J.F., 2020. Tectono-Stratigraphic Evolution of the Atuel Depocenter During the Late Triassic to Early Jurassic Rift Stage, Neuquén Basin, West-Central Argentina. In: Kietzmann D., Folguera A. (eds) Opening and Closure of the Neuquén Basin in the Southern Andes. Springer Earth System Sciences. Springer, Cham.

Bernet, M., Spiegel, C., 2004. Detrital thermochronology: Provenance analysis, exhumation, and landscape evolution of mountain belts (Vol. 378). Geological Society of America.

Bernet, M., 2019. Exhumation studies of mountain belts based on detrital fission-track analysis on sand and sandstones. In: Fission-track thermochronology and its application to geology (pp. 269-277). Springer, Cham.

Borghi, P., Fennell, L., Omil, R.G., Naipauer, M., Acevedo, E., Folguera, A., 2019. The Neuquén Group: The reconstruction of a Late Cretaceous foreland basin in the southern Central Andes (35–37°S). Tectonophysics 767, 228177. https://doi.org/10.1016/j.tecto.2019.228177.

Boyce, D.I., Charrier, R., Tapia, F., Farías, M., 2014. Mid-Cretaceous Compressive Deformation in Central Chile: The Beginning of the Andean Building (In AGU Fall Meeting Abstracts).

Boyce, D., Charrier, R., Farías, M., 2020. The first Andean compressive tectonic phase. Sedimentologic and structural analysis of mid- Cretaceous deposits in the

Coastal Cordillera, Central Chile (32°50’S). Tectonics. doi:10.1029/2019tc005825

Buelow, E.K., Suriano, J., Mahoney, J.B., Kimbrough, D.L., Mescua, J.F., Giambiagi, L.B., Hoke, G.D., 2018. Sedimentologic and stratigraphic evolution of the Cacheuta basin: Constraints on the development of the Miocene retroarc foreland basin, south-central Andes. Lithosphere 10 (3): 366–391. doi: https://doi.org/10.1130/L709.1.

Brandon, M. T., 2002. Decomposition of mixed grain age distributions using Binomfit. On Track, 24, 13–18.

Brandon, M. T., Roden-Tice M. K., Garver J. I., 1998. Late Cenozoic exhumation of the Cascadia accretionary wedge in the Olympic Mountains, Northwest Washington State: Geological Society of America Bulletin, v. 110, no. 8, p. 985B1009.

Bridge, J.S., 2003. Rivers and floodplains: forms, processes and sedimentary record. Blackwell, Oxford, 491 p.

Broens, S., Pereira, M., 2005. Evolución estructural de la zona de transición entre las fajas plegadas y corridas de Aconcagua y Malargüe, Provincia de Mendoza. Revista de la Asociación Geológica Argentina 60 (4): 685-695.

Cain, S.A., Mountney, N.P., 2009. Spatial and temporal evolution of a terminal fluvial fan system: the Permian Organ Rock Formation, South-east Utah. Sedimentology 56: 1774-1800.

Carrapa, B., 2010. Resolving tectonic problems by dating detrital minerals. Geology 38 (2), 191–192.

Carrapa, B., DeCelles, P.G., Reiners, P.W., Gehrels, G.E., Sudo, M., 2009. Apatite triple dating and white mica $^{40}Ar/^{39}Ar$ thermochronologyof syntectonic detritus in the Central Andes: A multiphase tectonothermal history. Geology 37 (5), 407–410.

Cawood, P.A., Hawkesworth, C.J., Dhuime, B., 2012. Detrital zircon record and tectonic setting. Geology 40 (10): 875–878. doi: https://doi.org/10.1130/G32945.1

Cazau, L.B., Uliana, M.A., 1973. El Cretácico Superior continental de la Cuenca neuquina. In: 5° Congreso Geológico Argentino (Carlos Paz, 1972), Actas 3, pp. 131–163 Buenos Aires.

Cecil, C.B., 2003. The concept of autocyclic and allocyclic controls on sedimentation and stratigraphy, emphasizing the climatic variable. Pages 13–20 in CB Cecil, NT Edgar, eds. Climate controls on stratigraphy, Vol 77. Society for Sedimentary Geology.

Charrier, R., Wyss, A.R., Flynn, J.J., Swisher, C.C., Norell, M.A., Zapatta, F., McKenna, M.C., Novacek, M.J., 1996. New evidence for Late Mesozoic-Early Cenozoic evolution of the Chilean Andes in the Upper Tinguiririca Valley (35°S), central Chile. Journal of South American Earth Sciences 9 (5-6), 393-422.

Charrier, R., Pinto, L., Rodríguez, M.P., 2007. Tectonostratigraphic evolution of the Andean Orogen in Chile. In: Moreno T, Gibbons W (Eds), The Geology of Chile. The Geological Society, London, pp 21–114.

Charrier, R., Ramos, V., Tapia, F., Sagripanti, L., 2015. Tectono-stratigraphic evolution of the Andean Orogen between 31 and 37°S (Chile and Western Argentina). In: Sepúlveda, S.A., Giambiagi, L.B., Moreiras, S.M., Pinto, L., Tunik, M., Hoke, G.D., Farías, M. (Eds.), Geodynamic Processes in the Andes of Central Chile and Argentina. Geological Society Special Publication. 399:13-61

Chen, Y.W., Wu, J., Suppe, J., 2019. Southward propagation of Nazca subduction along the Andes. Nature 565 (7740), 441.

Chew, D.M., Donelick, R.A., 2012. Combined apatite fission track and U-Pb dating by LA-ICP-MS and its application in apatite provenance analysis. Quantitative mineralogy and microanalysis of sediments and sedimentary rocks. Mineralogical Association of Canada, Short Course 42, 219–247.

Cobbold, P.R., Rossello, E.A., 2003. Aptian to recent compressional deformation of the Neuquén Basin, Argentina. Marine and Petroleum Geology 20, 429-443.

Contreras J.P, Schilling M.E., Geología del área San Fernando - Curicó, regiones del Libertador General Bernardo O´Higgins y del Maule, Escala 1:100.000, in: Carta Geológica de Chile, Serie Geológica Básica. SERNAGEOMIN, p 50 (In Press).

Corbella, H., Novas, F.E., Apesteguía, S., Leanza, H.A., 2004. First fission track-age for the dinosaur-bearing Neuquén Group (Upper Cretaceous) Neuquén Basin, Argentina. Revista Museo Argentino de Ciencias Naturales 6 (2), 1–6 (n.s).

Cox, E.P., 1927. A method of assigning numerical and percentage values to the degree of roundness of sand grains. Journal of Paleontology 1(3), 179–183.

Coutts, D.S., Matthews, W.A., Hubbard, S.M., 2019. Assessment of widely used methods to derive depositional ages from detrital zircon populations. Geoscience Frontiers 10(4), 1421–1435.

Cristallini, E.O., Ramos, V.A., 1996. Los depósitos continentales Cretácicos y volcanitas asociadas. In: Aguirre-Urreta, M.B., Alvarez, P.P., Cegarra, M., Cristallini, E.O., Kay, S.M., Lo Forte, G.L., Pereyra, F.X., Perez, D.J. (Eds.), Geología de La Región Del Aconcagua, Provincias de San Juan Y Mendoza, República Argentina. Direccion Nacional del Servicio Geologico, Buenos Aires, pp. 231–273.

Critelli, S., Ingersoll, R.V., 1995. Interpretation of neovolcanic versus palaeovolcanic sand grains: an example from Miocene deep-marine sandstone of the Topanga Group (Southern California). Sedimentology 42, 783–804.

Critelli, S., Nilsen, T.H., 2000. Provenance and stratigraphy of the Eocene Tejon Formation, Western Tehachapi Mountains, San Emigdio Mountains, and southern San Joaquin Basin, California. Sedimentary Geology 136 (1-2), 7-27.

D'Elia, L., Bilme,s A., Naipauer, M., Vergani, G.D., Muravchik, M., Franzese, J.R., 2020. The Syn-Rift of the Neuquén Basin (Precuyano and Lower Cuyano Cycle): Review of Structure, Volcanism, Tectono-Stratigraphy and Depositional Scenarios. In: Kietzmann D., Folguera A. (eds) Opening and Closure of the Neuquén Basin in the Southern Andes. Springer Earth System Sciences. Springer, Cham.

Di Giulio, A., Ronchi, A., Sanfilippo, A., Balgord, E., Carrapa, B., Ramos, V.A., 2017. Cretaceous evolution of the Andean margin between 36°S and 40°S latitude through a multi-proxy provenance analysis of Neuquén Basin strata (Argentina). Basin Research 29, 284–304.

Di Giulio, A., Ronchi, A., Sanfilippo, A., Tiepolo, M., Pimentel, M., Ramos, V.A., 2012. Detrital zircon provenance from the Neuquén Basin (south-central Andes):

Cretaceous geodynamic evolution and sedimentary response in a retroarc-foreland basin. Geology 40, 559–562.

Dickinson, W.R., Beard, L.S., Brakenridge, G.R., Erjavec, J.L., Ferguson, R.C., Inman, K.F., Knepp, R.A., Lindberg, F.A., Ryberg, P.T., 1983. Provenance of North American Phanerozoic sandstones in Relation to Tectonic Setting. Geological Society of America, Bulletin 94, pp. 222–235.

Dickinson, W.R., Gehrels, G.E., 2009. Use of U-Pb ages of detrital zircons to infer maximum depositional ages of strata: a test against a Colorado Plateau database. Earth and Planetary Science Letters 288 (1–2), 115–125. https://doi.org/10.1016/j.epsl.2009.09.013.

Dickson, J.A.D., 1965. A modified staining technique for carbonates in thin section. Nature 205 (4971) 587-587.

Dingus, L., Clarke, J., Scott, G.R., Swisher, C.C., Chiappe, L.M., Coria, R.A., 2000. Stratigraphy and magnetostratigraphic/faunal constrains for the age of sauropod embryo-bearing rocks in the Neuquén Group (Late Cretaceous, Neuquén province, Argentina). American Museum novitates 3290, 1–11.

Dunkl, I., 2002. TRACKKEY: a Windows program for calculation and graphical presentation of fission track data. Computers and Geosciences, 28 (1), 3-12.

Faccenna, C., Oncken, O., Holt, A.F., Becker, T.W., 2017. Initiation of the Andean orogeny by lower mantle subduction. Earth and Planetary Science Letters 463, 189–201.

Fedo, C.M., 2003. Detrital zircon analysis of the sedimentary record. Reviews in Mineralogy and Geochemistry 53, 277–303.

Fennell, L., Folguera, A., Naipauer, M., Gianni, G., Rojas Vera, E., Bottesi, G., Ramos, V.A., 2017a. Cretaceous deformation of the southern Central Andes: synorogenic growth strata in the Neuquén Group (35°30′–37°S). Basin Research 29, 51–72.

Fennell, L., Naipauer, M., Folguera, A., 2017b. El movimiento Intersenoniano de Pablo Groeber en el norte de Neuquén y Sur de Mendoza: bases de la primera orogenia andina. Revista de la Asociación Geológica Argentina; Año: 2017 74, 59–73.

Fennell, L., Naipauer, M., Borghi, P., Sagripanti, L., Pimentel, M., Folguera A., 2020. Early Jurassic intraplate extension in west-central Argentina constrained by U-Pb SHRIMP dating: Implications for the opening of the Neuquén basin. Gondwana Research 87, 278-302.

Finzel, E. S., 2017. Detrital zircon microtextures and U- PB geochronology of Upper Jurassic to Paleocene strata in the distal North American Cordillera foreland basin, Tectonics 36, 1295– 1316. doi:10.1002/2017TC004549.

Fleischer, R.L., Price P.B., Walker R.M., 1975. Nuclear Tracks in Solids: Principles and Applications. University of California Press, Berkeley.

Folk, R.L., Andrews, P.B., Lewis, D.W., 1970. Detrital sedimentary rock classification and nomenclature for use in New Zeland. N.Z. Journal of Geology and Geophysics 13, 937–968.

Franklin, J., Tyrrell, S., Morton, A.C., Frei, D., Mark, C., 2019. Triassic sand supply to the Slyne Basin, offshore western Ireland – new insights from a multi-proxy provenance approach. Journal of the Geological Society 176, 1120 - 1135.

Fuentes, F., Horton, B., Starck, D., Boll, A., 2016. Structure and tectonic evolution of hybrid thick- and thin-skinned systems in the Malargüe fold–thrust belt, Neuquén basin, Argentina. Geological Magazine, 153(5-6), 1066-1084. doi:10.1017/S0016756816000583

Gabriele, N.A., 2016. Evapofacies del Miembro Troncoso Superior de la Formación Huitrín (Cretácico Inferior, Cuenca Neuquina, Argentina): paleoambientes, evolución y controles. Latin American Journal of Sedimentology and Basin Analysis 23 (1):35-69.

Galbraith, R. F., 1981. On statistical models for fission track counts. Journal of the International Association for Mathematical Geology, 13 (6), 471-478.

Galbraith, R.F., Green P.F., 1990. Estimating the component ages in a finite mixture. Nuclear Tracks and Radiation Measurements, 17(3), 197–206. https://doi.org/10.1016/1359-0189(90)90035-V.

Galetto, A., Georgieva, V., García, V. H., Zattin, M., Sobel, E. R., Glodny, J., Bordese, S., Arzadún, G., Bechis, F., Caselli, A. T., Becchio, R., 2021. Cretaceous and Eocene rapid cooling phases in the Southern Andes (36°–37°S): Insights from low-temperature thermochronology, U-Pb geochronology, and inverse thermal modeling from Domuyo area, Argentina. Tectonics, https://doi.org/10.1029/2020TC006415

Garrido, A.C., 2010. Estratigrafía del Grupo Neuquén, Cretácico Superior de la Cuenca Neuquina (República Argentina): nueva propuesta de ordenamiento litoestratigráfico. Revista del Museo Argentino de Ciencias Naturales. Nueva Serie 12 (2).

Garver, J.I., Brandon, M.T., Roden-Tice, M., Kamp, P.J., 1999. Exhumation history of orogenic highlands determined by detrital fission-track thermochronology. Geological Society, London, Special Publications, 154(1), 283-304.

Gehrels, G., 2014. Detrital zircon U-Pb geochronology applied to tectonics. Annual Review of Earth and Planetary Sciences, 42 , pp. 127-149.

Gehrels, G.E., Valencia, V., Pullen, A., 2006. Detrital zircon geochronology by laser–ablation multicollector ICPMS at the Arizona LaserChron center. In: Olszewski, T., Huff, W. (Eds.), Geochronology: Emerging Opportunities, Paleontological Society Short Course, October 21, 2006, Philadelphia, PA, vol. 12. pp. 1–10 Paleontological Society.

Gehrels, G.E., Valencia, V., Ruiz, J., 2008. Enhanced precision, accuracy, efficiency, and spatial resolution of U- Pb ages by laser ablation– multicollector inductively coupled plasma–mass spectrometry. Geochemistry, Geophysics, Geosystems 9, Q03017. https://doi.org/ 10.1029/2007GC001805.

Ghiglione, M., Naipauer, M., Sue, C., Barberón, V., Valencia, V., Aguirre-Urreta, B., Ramos, V., 2015. U-Pb zircon ages from the northern Austral basin and their correlation with the Early Cretaceous exhumation and volcanism of Patagonia. Cretaceous Research 55; 7-2015; 116-128.

Giambiagi, L., Bechis, F., García, V., Clark, A.H., 2008. Temporal and spatial relationships of thick- and thin-skinned deformation: A case study from the Malargüe fold-and-thrust belt, southern Central Andes. Tectonophysics, 459(1-4), 123-139.http://dx.doi.org/10.1016/j.tecto.2007.11.069

Giambiagi, L., Ghiglione, M., Cristallini, E., Bottesi, G., 2009. Kinematic models of basement/cover interaction: Insights from the Malargüe fold and thrust belt, Mendoza, Argentina. Journal of Structural Geology, 31(12), 1443-1457. http://dx.doi.org/10.1016/j.jsg.2009.10.006

Gianni, G.M., Navarrete, C., Echaurren, A., Díaz, M., Butler, K.L., Horton, B.K., Encinas, A., Folguera, A., 2020. Northward propagation of Andean genesis: Insights from Early Cretaceous synorogenic deposits in the Aysén-Río Mayo basin. Gondwana Research 77, 238–259. https://doi.org/10.1016/j.gr.2019.07.014.

Gibling, M.R., 2006. Width and thickness of fluvial channel bodies and valley fills in the geological record: a literature compilation and classification. Journal of Sedimentary Research 76:731–770.

Gleadow, A.J.W., Fitzgerald P.G., 1987. Uplift history and structure of the Transantarctic mountains-New evidence from fission-track dating of basement apatites in the Dry Valleys area, southern Victoria Land, Earth and Planetary Science Letters 82, 1-14.

Godoy, E., Schilling, M., Solari, M., Fock, A., 2009. Geología del área Rancagua-San Vicente de Tagua-Tagua, Región del Libertador Bernardo O'Higgins. Carta Geológica de Chile, Serie Geológica Básica No. 118. Servicio Nacional de Geología y Minería, Santiago.

Gómez, R., Lothari, L., Tunik, M., Casadio, S., 2019. Onset of foreland basin deposition in the Neuquén Basin (34°-35°S): New data from sedimentary petrology and U–Pb dating of detrital zircons from the Upper Cretaceous non-marine deposits.

Journal of South American Earth Science 95, 102257. https://doi.org/10.1016/j.jsames.2019.102257.

Gómez, R., Tunik, M. A., Casadío, S. A., 2020. Fluvial deposits as a record of the Late Cretaceous tectonic activity in southern Central Andes, Argentina. Servicio Nacional de Geología y Minería; Andean Geology 47 (2); 256-274.

Hartley, A.J., Weissmann, G.S., Nichols, G.J., Warwick, G.L., 2010. Large distributive fluvial systems: characteristics, distribution and controls on development. Journal of Sedimentary Research 80: 167-183. doi: 10.2110/jsr.2010.016.

Horton, B.K., 2018. Tectonic Regimes of the Central and Southern Andes: Responses to Variations in Plate Coupling During Subduction. Tectonics 402–429. https://doi.org/10.1002/2017TC004624.

Howell, J.A., Schwarz, E., Spalletti, L., Veiga, G.D., 2005. The Neuquén Basin: an overview. In: Veiga, G. (Ed.), The Neuquén Basin: a Case Study in Sequence Stratigraphy and Basin Dynamics: the Geological Society, vol. 252. Special Publication, pp. 1–14.

Hurford, A.J., Green, P.F., 1983. The zeta age calibration of fission-track dating. Chemical Geology 41, 285-317.

Ingersoll, R.V., Fullard, T.F., Ford, R.L., Grimm, J.P., Pickle, J.D., Sares, S.W., 1984. The effect of grain size on detrital modes; a test of the Gazzi–Dickinson point-counting method. Journal of Sedimentary Research 54, 103–116.

Ketcham, R.A., Donelick, R.A., Carlson, W.D., 1999. Variability of apatite fission-track annealing kinetics: III. Extrapolation to geological time scales. American Mineralogist 84 (9), 1235-1255. https://10.2138/am-1999-0903.

Kozlowski, E., Manceda, R., Ramos, V.A., 1993. Estructura. In: Ramos V.A., (Eds.) Geología y Recursos Naturales de Mendoza. Asociación geológica Argentina, Buenos Aires, 235–256.

Laslett, G. M., Green, P.F., Duddy, I.R., Gleadow, A.J.W., 1987. Thermal annealing of fission tracks in apatite 2. A quantitative analysis. Chemical Geology 65, 1-13.

Lazo, D.G., Cataldo, C.S., Luci, L., Aguirre-Urreta M.B., 2017. Groeber y los invertebrados fósiles del Miembro La Tosca, Cretácico Inferior de la Cuenca Neuquina: una historia de controversias paleontológicas. Revista de la Asociación Geológica Argentina 74:9–39.

Leanza, H.A., 2003. Las sedimentitas huitrinianas y rayosianas (Cretácico Inferior) en el ámbito central y meridional de la cuenca Neuquina, Argentina. Servicio Geológico Minero Argentino, Serie Contribuciones Técnicas-Geología, Buenos Aires, 1–31.

Leanza, H.A., 2009. Las principales discordancias del Mesozoico de la Cuenca Neuquina según observaciones de superficie. Revista del Museo Argentino de Ciencias Naturales. Nueva Serie 11 (2), 145–184.

Leanza, H.A., Apesteguía, S., Novas, F.E., de la Fuente, M.S., 2004. Cretaceous terrestrial beds from the Neuquén Basin (Argentina) and their tetrapod assemblages. Cretaceous Research 25, 61–87.

Leanza, H.A., Hugo, C.A., 2001. Hoja Geológica 3969-I - Zapala, provincia del Neuquén. Instituto de Geología y Recursos Naturales. SEGEMAR. Boletín 275, 1–128 Buenos Aires.

Legarreta L., Uliana, M.A., 1996. The Jurassic succession in west-central Argentina: stratal pattern, sequences and paleogeographic evolution. Palaeogeography, Palaeoclimatology, Palaeoecology 120:303–330.

Legarreta, L., Gulisano, C.A., 1989. Análisis estratigráfico secuencial de la Cuenca Neuquina (Triásico superior - terciario inferior). In: En, Chebli, G., Spalletti, L. (Eds.), Cuencas Sedimentarias Argentinas. X° Congreso Geológico Argentino. Serie Correlación Geológica, vol. 6. pp. 221–243 Buenos Aires.

Lothari, L., Gómez, R., Tunik, M., Casadio, S., 2020. Análisis de facies y petrografía de los depósitos del Cretácico Superior en el norte de la cuenca Neuquina: implicancias para el inicio de la etapa de foreland. Latin American Journal of Sedimentology and Basin Analysis 27 (1), 3-28.

Lowe, D.R., 1982. Sediment gravity flows: II . Depositional models with special reference to the deposits of highdensity turbidity currents. Journal of Sedimentary Petrology 52: 279-297.

Mackaman-Lofland, C., Horton, B.K., Fuentes, F., Constenius, K.N., Stockli, D.F., 2019. Mesozoic to Cenozoic retroarc basin evolution during changes in tectonic regime, southern Central Andes (31–33°S): Insights from zircon UPb geochronology. Journal of South American Earth Sciences. doi: 10.1016/j.jsames.2018.10.004.

Manceda R., Figueroa D., 1995. Inversion of the Mesozoic Neuquén rift in the Malargüe fold and thrust belt, Mendoza, Argentina. In: Tankard AJ, Suárez Soruco R, Welsink HJ (Eds.) Petroleum Basins of South America. AAPG Memoir 62:369–382.

Martos, F., Fennell, L., Brisson, S., Palmieri, G., Naipauer, M., Folguera, A., 2020 Tectonic evolution of the northern Malargüe Fold and Thrust Belt, Mendoza province, Argentina. Journal of South American Earth Sciences, doi: https://doi.org/10.1016/j.jsames.2020.102711.

Matthews, K.J., Seton, M., Müller, R.D., 2012. A global-scale plate reorganization event at 105−100 Ma. Earth and Planetary Science Letters, 355, 283-298.

Méndez, V.E., Zappettini, E., Zanettini, J.C., 1995. Geología y metalogénesis del Orógeno Andino Central, República Argentina. Secretaría de Minería. 23: 1-190. Buenos Aires.

Mescua, J., Giambiagi, L.B., Ramos, V.A., 2013. Late cretaceous uplift in the Malargüe fold-and-thrust belt (35°S), southern central Andes of Argentina and Chile. Andean Geology 40, 102–116.

Miall A.D., 1985. Architectural-element analysis: a new method of facies analysis applied to fluvial deposits. Earth-Science Reviews 22:261–308.

Miall A.D., 1996. The geology of fluvial deposits: sedimentary facies, basin analysis and petroleum geology. Springer-Verlag, Inc., Heidelberg, 582 p.

Miall, A.D., 2014. Fluvial Depositional Systems. Springer: 316 p. New York.

Malusà, M.G, Villa, I.M., Vezzoli, G., Garzanti, E., 2011. Detrital geochronology of unroofing magmatic complexes and the slow erosion of Oligocene volcanoes in the Alps. Earth and Planetary Science Letters 301: 324–336.

Malusà, M.G., Fitzgerald, P.G., 2019. Application of thermochronology to geologic problems: bedrock and detrital approaches. In Fission-Track Thermochronology and its Application to Geology (pp. 191-209). Springer, Cham.

Malusà, M.G., Fitzgerald, P. G., 2019. From cooling to exhumation: setting the reference frame for the interpretation of thermochronologic data. In Fission-Track Thermochronology and its Application to Geology (pp. 147-164). Springer, Cham.

Mosquera, A., 2008. Mecánica de deformación de la Cuenca Neuquina (Triásico-Terciario). Ph.D. thesis, Universidad de Buenos Aires.

Mpodozis, C., Ramos, V., 1990. The Andes of Chile and Argentina, in: Cañas Pinochet, M.., Reinemud, J.. (Eds.), Geology of the Andes and Its Relation to Hydrocarbon and Mineral Resources. Circum Pacific Council Publications, Houston, pp. 59–90.

Mpodozis, C., Ramos, V.A., 2008. Tectónica Jurásica en Argentina y Chile: extensión, subducción oblicua, rifting, deriva y colisiones? Revista de la Asociación Geológica Argentina 63(4):481–497.

Müller, R.D., Seton, M., Zahirovic, S., Williams, S.E., Matthews, K.J., Wright, N.M., Shephard, G.E., Maloney, K.T., Barnett-Moore, N., Hosseinpour, M., Bower, D.J., Cannon, J., 2016. Ocean basin evolution and global-scale plate reorganization events since Pangea breakup, Annual Review of Earth and Planetary Sciences, Vol 44, 107-138. DOI: 10.1146/annurev-earth-060115-012211.

Muñoz, M., Tapia, F., Persico, M., Benoit, M., Charrier, R., Farías, M., Rojas, A., 2018. Extensional tectonics during Late Cretaceous evolution of the southern Central Andes: evidence from the Chilean main range at ~35°S. Tectonophysics. https://doi.org/10.1016/j.tecto.2018.06.009.

Mutti, E., 1992. Turbidite sandstone. Instituto di Geologia Universita di Parma, Azienda Generale Italiana Petroli, Milano: 275 p. San Donato Milanese.

Naipauer M., García Morabito, E., Manassero, M., Valencia, V.V., Ramos, V.A., 2018. A Provenance Analysis from the Lower Jurassic Units of the Neuquén Basin. Volcanic Arc or Intraplate Magmatic Input?. In: Folguera A. et al., (Eds). The Evolution of the Chilean-Argentinean Andes. Springer Earth System Sciences. Springer, Cham.

Naipauer, M., Ramos, V.A., 2016. Changes in Source Areas at Neuquén Basin: Mesozoic evolution and tectonic setting based on U–Pb ages on zircons. In: Folguera A, Naipauer M, Sagripanti L., et al (Eds.) Growth of the Southern Andes. Springer Earth System Sciences, Switzerland, pp 1–269.

Nichols, G.J., Fisher, J.A., 2007. Processes, facies and architecture of fluvial distributary system deposits. Sedimentary Geology 195 (1): 75-90.

North, C.P., Warwick, G.L., 2007. Fluvial Fans: Myths, Misconceptions, and the End of the Terminal-Fan Model. Journal of Sedimentary Research 77 (9): 693-701.

Oliveros, V., Féraud, G., Aguirre, L., Morata, D., 2006. The Early Andean Magmatic Province (EAMP): $^{40}Ar/^{39}Ar$ dating on Mesozoic volcanic and plutonic rocks from the Coastal Cordillera, Northern Chile. Journal of Volcanological and Geothermal Research 157: 311-330.

Oliveros, V., González, J., Espinoza, M., Vásquez, P., Rossel, P., Creixell, C., Sepúlveda, F., Bastías, F., 2018. The early stages of the Magmatic Arc in the Southern Central Andes. In: Folguera A, Contreras Reyes E et al (eds) The evolution of the Chilean-Argentinean Andes. Springer, Cham, pp 165–190.

Orts, D.L., Folguera, A., Giménez, M., Ramos, V.A., 2012. Variable structural controls through time in the southern central Andes (~36°S). Andean Geology 39 (2), 220–241.

Owusu Agyemang, P.C., Roberts, E.M., Bussert, R., Evans, D., Müller, J., 2019. U–Pb detrital zircon constraints on the depositional age and provenance of the dinosaur-bearing Upper Cretaceous Wadi Milk Formation of Sudan. Cretaceous Research 97, 52–72.

Paredes, J.M., Foix, N., Allard, J.O., Valle, M.N., Giordano, S.R., 2018. Complex alluvial architecture, paleohydraulics and controls of a multichannel fluvial system: Bajo Barreal Formation (Upper Cretaceous) in the Cerro Ballena anticline, Golfo San Jorge Basin, Patagonia. Journal of South American Earth Sciences. doi: 10.1016/j.jsames.2018.05.007.

Peyton, L. S., Carrapa B., 2013. An introduction to low-temperature thermochronologic techniques, methodology, and applications, in C. Knight and J. Cuzella, eds., Application of structural methods to Rocky Mountain hydrocarbon exploration and development: AAPG Studies in Geology 65, p. 15–36.

Potter, P.E., Pettijohn, F.J., 1977. Paleocurrents and basin analysis: New York, Springer-Verlag, 425 p.

Price, P. B., Walker R. M., 1963. Fossil tracks of charged particles in mica and the age of minerals. Journal Geophysics Research 68, 4847-4862.

Ramos, V., 1988. The tectonics of the Central Andes: 30°-33°S latitude. In: Clark, S., Burchfield, D. (Eds.), Processes in Continental Lithosferic Deformation, vol. 218. Geological Society of America, pp. 31e54. Special Papers.

Ramos, V.A., 1981. Descripción geológica de la Hoja 33c Los Chihuidos Norte, Provincia del Neuquén. Servicio Geológico Nacional, Boletín, vol. 182. pp. 1–103 Buenos Aires.

Ramos, V.A., 2009. Anatomy and global context of the Andes: Main geologic features and the Andean orogenic cycle. Backbone of the Americas: Shallow Subduction, Plateau Uplift, and Ridge and Terrane Collision, 204, 31-65.

Ramos, V.A., 2010. The tectonic regime along the Andes: Present settings as a key for the Mesozoic regimes. Geological Journal 45, 2-25.

Ramos, V.A, Folguera A., 2005. Tectonic evolution of the Andes of Neuquén: constraints derived from the magmatic arc and foreland deformation. In: Veiga GD, Spalletti L.A., Howell J.A., Schwarz E., (Eds.) The Neuquén Basin, Argentina: a case study in sequence stratigraphy and basin dynamics. Geological Society, London, SP 252:15–35

Ramos, V.A., Kay S.M., 2006. Overview of the tectonic evolution of the southern Central Andes of Mendoza and Neuquén (35°–39° S latitude). In: Kay S.M., Ramos V.A., (Eds.). Evolution of an Andean margin: a tectonic and magmatic view from the Andes to the Neuquén Basin (35°–39°S). Geological Society of America, SP 407, pp 1–17.

Rahl, J.M., Ehlers, T.A., Van der Pluijm, B.A., 2007. Quantifying transient erosion of orogens with detrital thermochronology from syntectonic basin deposits. Earth and Planetary Science Letters 256:147–161.

Rossel, P., Oliveros, V., Mescua, J., Tapia, F., Ducea, M.N., Calderón, S., Charrier, R., Hoffman, D., 2014. El volcanismo Jurásico Superior de la Formación Río Damas-Tordillo (33°-35,5°S): antecedentes su sobre petrogénesis, cronología, proveniencia e implicancias tectónicas. Andean Geology 41, 529–557. https://doi.org/10.5027/andgeoV41n3-a03.

Roulston B.V., Waugh, D.C., 1983. Stratigraphic comparison of the Mississippian Potash Deposits in New Brunswick, Canada. En B.Ch. Schreiber y H. L. Harner (Eds.), Sixth International Symposium on Salt. T.I: 115-129. The Salt Institute, Alexandria, VA.

Sánchez, M., Rossi, J., Morra, S., Armas, P., 2008. Análisis estratigráfico secuencial de las Formaciones Huincul y Lisandro del Subgrupo Río Limay (Grupo Neuquén-Cretácico Superior) en el departamento El Cuy, Río Negro, Argentina. Latin American Journal of Sedimentology and Basin Analysis 15 (1), 1-26.

Sánchez, M.L., Asurmendi, E., Armas, P., 2013. Subgrupo Río Colorado (Grupo Neuquén): registros de paleosismidad en la cuenca de antepaís andina, Cuenca Neuquina, Provincias de Neuquén y Río Negro, Argentina. Revista de la Asociación Geológica Argentina 70 (1), 96-114.

Sato, A.M., Llambías, E.J., Basei, M.A.S., Castro, C.E., 2015. Three stages in the Late Paleozoic to Triassic magmatism of southwestern Gondwana, and the relationships with the volcanogenic events in coeval basins. Journal of South

American Earth Science 63, 48–69. https://doi.org/10.1016/j.jsames.2015.07.005.

Schellart, W. P., 2008. Overriding plate shortening and extension above subduction zones: A parametric study to explain formation of the Andes Mountains. Geological Society of America Bulletin, 120, 11-12, 1441-1454.

Schellart, W.P., 2017. Andean mountain building and magmatic arc migration driven by subduction-induced whole mantle flow. Nature Communications 8 (1), 2010.

Schumm, S.A., 1981. Evolution and response of the fluvial system, sedimentological implications. In: Ethridge FG, Flores RM (eds) Recent and ancient nonmarine depositional environments: models for exploration, vol. 31. Society of Economic Paleontologists and Mineralogists, Special Publication, pp 19–29.

Schwarz, E., Spalletti, L.A., Veiga, G.D., Fanning, C.M., 2016. First U-Pb SHRIMP age for the Pilmatué Member (Agrio Formation) of the Neuquén Basin, Argentina: Implications for the Hauterivian lower boundary. Cretaceous Research 58; 3-2016; 223-233.

Slingerland, R.L., Smith, N.D., 2004. River avulsions and their deposits: Annual Revisions of Earth and Planetary Science, 32: 257-285.

Somoza, R., Zaffarana, C.B., 2008. Mid-Cretaceous Polar Standstill of South America, Motion of the Atlantic Hotspots and the Birth of the Andean Cordillera. Earth and Planetary Science Letters 271, 267–277.

Suriano, J., Mardonez, D., Mahoney, J.B., Mescua, J.F., Giambiagi, L.B., Kimbrough, D., Lossada, A., 2017. Uplift sequence of the Andes at 30°S: insights from sedimentology and U/Pb dating of synorogenic deposits. Journal of South American Earth Sciences vol. 75, p. 11-34.

Surpless, K.D., Augsburger, G.A., 2009. Provenance of the Pythian Cave conglomerate, northern California: implications for mid-Cretaceous paleogeography of the U.S. Cordillera. Cretaceous Research 30, 1181-1192.

Tagami, T., 2005. Zircon fission-track thermochronology and applications to fault studies. Reviews in Mineralogy and Geochemistry, 58(1), 95-122.

Tapia, F., Muñoz, M., Farías, M., Charrier, R., Astaburuaga, D., 2020. Middle Jurassic-Late Cretaceous Paleogeography of the Western Margin of the Neuquén Basin (34° 30′–36° S). In: Kietzmann D., Folguera A., (Eds.) Opening and Closure of the Neuquén Basin in the Southern Andes. Springer Earth System Sciences. Springer, Cham.

Thomson, K.D., Stockli, D.F., Clark, J.D., Puigdefàbregas, C., Fildani, A., 2017. Detrital zircon (U-Th)/(He-Pb) double-dating constraints on provenance and foreland basin evolution of the Ainsa Basin, south-central Pyrenees, Spain, Tectonics 36.

Tucker, R.T., Roberts, E.M., Hu, Y., Kemp, A.I., Salisbury, S.W., 2013. Detrital zircon age constraints for the Winton formation, Queensland: Contextualizing Australia’s late Cretaceous dinosaur faunas. Gondwana Research 24, 767e779.

Tunik, M.A., 2001. Análisis sedimentológico y tectónico de la primera ingresión atlántica en la Alta Cordillera de Mendoza. Tesis doctoral (inédito). Facultad de Ciencias Exactas y Naturales, Universidad de Buenos Aires. pp. 257.

Tunik, M.A., 2003. Interpretación paleoambiental de los depósitos de la Formación Saldeño (Cretácico superior), en la alta Cordillera de Mendoza. Revista de la Asociación Geológica Argentina 58: 417-433.

Tunik, M.A., Concheyro, A., Ottone, G., Aguirre-Urreta, M.B., 2004. Paleontología de la Formación Saldeño (Maastrichtiano), Alta Cordillera de Mendoza, Argentina. Ameghiniana 41: 143-160.

Tunik, M., Folguera, A., Naipauer, M., Pimentel, M., Ramos, V., 2010. Early uplift and orogenic deformation in the Neuquén Basin: constraints on the Andean uplift from U–Pb and Hf isotopic data of detrital zircons. Tectonophysics 489, 258–273.

Turienzo, M., 2010. Structural style of the Malargüe fold and-thrust belt at the Diamante river area (34° 30–34° 50 S) and its linkage with the Cordillera frontal Andes of central Argentina. Journal of South American Earth Science 29:537–556.

Turienzo, M., Dimieri, L., Frisicale, C., Araujo, V., Sanchéz, N., 2012. Cenozoic structural evolution of the Argentinean Andes at 34°40’S: A close relationship between thick and thin-skinned deformation. Andean Geology 39. https://doi.org/10.5027/andgeov39n2-a07.

Tyrrell, S., Haughton, P.D.W., Daly, J.S., Shannon, P.M., 2012. The Pb isotopic composition of detrital K-feldspar: a tool for constraining provenance, sedimentary processes and paleo-drainage. In: Sylvester, P., (Eds.) Quantitative Mineralogy and Microanalysis of Sediments and Sedimentary Rocks. Mineralogical Association of Canada Short Course Series, 42, 203-217.

Uliana, M.A., Legarreta L., 1993. Hydrocarbons habitat in a Triassic to Cretaceous sub-andean setting: Neuquén basin, Argentina. Journal of Petroleum Geology 16:397–420.

Uliana, M.A., Dellapé, D.A., 1981. Estratigrafía y evolución paleoambiental de la sucesión Maestrichtiano-Eoterciaria del engolfamiento neuquino (Patagonia septentrional). In: 8° Congreso Geológico Argentino (San Luis), Actas3, pp. 673–711.

Umazano, A.M., Bellosi, E.S., Visconti, G., Jalfin, G.A., Melchor, R.N., 2009. Sedimentary record of a Late Cretaceous volcanic arc in central Patagonia: petrography, geochemistry and provenance of fluvial volcaniclastic deposits of the Bajo Barreal Formation, San Jorge Basin, Argentina. Cretaceous Research 30; 3; 6-2009; 749-766.

Veiga, G.D., Vergani, G.D., 2011. El Miembro Troncoso Inferior de la Formación Huitrín (Cretácico Temprano). En H.A. Leanza, C. Arregui, O. Carbone, J.C. Danieli y J.M. Vallés (Eds.), Geología y Recursos Naturales de la Provincia del Neuquén. Relatorio del 18º Congreso Geológico Argentino: 181-188. Buenos Aires.

Vergani, G., Tankard, A.J., Belotti, H.J., Welsnik, H.J., 1995. Tectonic evolution and paleogeography of the Neuquén Basin, Argentina. In: Petroleum Basins of South America, vol. 62. AAPG Memoir, pp. 383–402. https://doi.org/10.1306/7834F6E1- 1721- 11D7-8645000102C1865D.

Vergara, M., Levi, B., Nystrom, J., Cancino, A., 1995. Jurassic and Early Cretaceous island arc volcanism, extension and subsidence in the Coast Range of central Chile. Geological Society of America Bulletin 107:1427-1440.

Vermeesch, P., 2012. On the visualisation of detrital age distributions. Chemical Geology v.312-313, 190-194, doi: 10.1016/j.chemgeo.2012.04.0210 .

Vermeesch, P., 2021. Maximum depositional age estimation revisited. Geoscience Frontiers 12(2), 843-850.

Weissmann, G.S., Hartley, A. J., Nichols, G.J., Scuderi, L.A., Olsen, M., Buehler, H., Banteah, R., 2010. Fluvial form in modern continental sedimentary basins: distributive fluvial systems. Geology 38:39-42.

Willner, A.P., Thomson, S.N., Kröner, A., Wartho, J., Wijbrans, J.R., Hervé, F., 2005. Time Markers for the Evolution and Exhumation History of a Late Palaeozoic Paired Metamorphic Belt in North–Central Chile (34°–35°30′S), Journal of Petrology, 46 (9) 1835–1858.

Zavala, C., Ponce, J., Drittanti, D., Arcuri, M., Freije, H., Asensio, M., 2006. Ancient lacustrine hyperpycnites: a depositional model from a case study in the Rayoso formation (Cretaceous) of west-central Argentina. Journal of Sedimentary Research 76, 41–59.

Figure captions

Figure 1. Regional DEM showing the location of the study area in the context of South America and the Neuquén Basin extension in the Jurassic-Cretaceous period. The main morphostructures are shown together with the maximum eastward progression of the Late Cretaceous orogenic front, and the extension of the Neuquén Group outcrops at present.

Figure 2. a) Local DEM of the study area with detail of the main morphostructures. b) Local geological map showing the main units, structural features and the location of stratigraphic sections (after Lothari et al., 2020). 1: Vega Grande; 2: Vega de Los Patos;

3: Arroyo Oscuro; 4: Arroyo Las Playas. Sections 1 and 2 correspond to the synthetic and schematic sections created by Gómez et al. (2019). Sections 3 and 4 belong to this work. c) Schematic sections of Vega Grande and Vega de Los Patos with the location of the samples collected for the provenance analysis (see Fig. 3 for the references) (after Gómez et al., 2019).

Figure 3. Measured stratigraphic section from the Arroyo Oscuro area.

Figure 4. Measured stratigraphic section from the Arroyo Las Playas area.

Figure 5. Photographs of the analysed outcrops. a) Conglomerate from Arroyo Las Playas section, composed almost exclusively of limestone rock fragments. b) Stacking of narrow to broad ribbon fluvial-channel deposits from the Arroyo Las Playas area. c) Outcrop view with: d) schematic panel depicting multiepisodic sandy-gravel channelized complex from the Arroyo Oscuro area. This architectural element shows paleoflow data and the typical sedimentary facies, as well as the hierarchy of the architectural units according to Miall (1996). e) Lateral view of the same outcrop showing the thickness of the fluvial macroform. f) Detail of the sedimentary facies.

Figure 6. a) AO01-17A sample. Photomicrographs of the framework's composition: monocrystalline quartz (Qm), plagioclase (Fpl), altered and undetermined lithic grain (La) and pyroclastic paleovolcanic lithic fragment (Lp) with eutaxitic textures. Calcite as a main type of cement (Cca). Photomicrographs on NP and NX. Scale: 100 µm. b) ALP06-17 sample. Photomicrographs of framework composition: monocrystalline quartz (Qm), altered and undetermined lithic grain (La), serial (Lps) paleovolcanic lithic fragment. Analcime as a type of zeolitic cement (Cc). Photomicrographs on NP and NX. Scale: 60 µm. c) AO08-17 sample. Photomicrographs of framework composition: high percentage of monocrystalline quartz (Qm) showing embayment, plagioclase (Fpl),

calcite cement (Cca) and different types of paleovolcanic lithic fragment. Photomicrographs on NX. Scale: 100 µm. d) ALP06-17 sample. Photomicrographs of framework composition: limestone lithic fragments (Lc), monocrystalline quartz (Qm), granular (Lpg) paleovolcanic lithic fragment, alkaline feldspar (Fk), altered and undetermined lithic grain (La), iron cement (Cf) and porosity (P). Photomicrographs on NP. Scale: 100 µm. d-e) ALP10-17 sample. Photomicrographs of framework composition: monocrystalline quartz (Qm), altered and undetermined lithic grain (La), serial (Lps) paleovolcanic lithic fragments and opaques (Op). These photomicrographs also show one rounded zircon grained (34.563 µ) and two apatite/zircon angular grained (50.755 and 29.470 µ). Photomicrographs on NP. Scale: 20 µm.

Figure 7. a) Sandstone classification QFL plot according to Folk et al. (1970) of the analysed samples. b) QFL and QmFLt plots of sandstones from Diamante Formation to discriminate provenance areas. On the left, QFL diagram from Dickinson et al. (1983). On the right, QmFLt from Dickinson et al. (1983). Q: total quartz, F: total feldspar, L: total lithic fragments, Qm: monocrystalline quartz, Lt: total lithic fragments plus polycrystalline quartz.

Figure 8. Graphical representation of AFT(I), ZFT(II) and U-Pb(III) data from samples VLP001 and 2119-Diamante. Fission track data is displayed by three different graphical devices: a- radial plot of single grain-ages; b-cumulative grain-age distribution; c- Kernel and probability density distributions. Plots a- and c- were made using a Density Plotter (Vermeesch, 2012). The U-Pb ages from analysed zircons are displayed with a frequency histogram and relative probability plot, focused on the youngest ages considering the correlation purpose (see Appendix 4 for complete plot and Gómez et al., 2019 for further details). In the I and III plots, the maximum depositional age of sample VLP001 is depicted with a dashed black line, and the AFT central age of the same sample is depicted

with a red shadow, including the range of analytical uncertainty. In the II plots, ZFT ages of discrete populations (P_1, P_2) from sample 2119-Diamante are indicated with continuous red and yellow lines, and the range of the analytical uncertainty is highlighted with the same colored shadow in each case.

Figure 9. Scanning Electron Microscope images (SEM) of apatite grains from the VLP001 sample showing the morphological classification proposed. a) Angular. b) Subangular. c) Rounded. The bar in each image represents 20 µm.

Figure 10. Scanning Electron Microscope images (SEM) of zircon grains from the VLP001 sample showing the morphological classification proposed. a) Angular. b) Subangular. c) Rounded. The bar in each image represents 20 µm.

Figure 11. Schematic block diagrams (unscaled) illustrating a paleogeographic reconstruction of the Andean Orogen (34-35°S). a) Early Cretaceous (Aptian) backarc stage showing the final disconnection of paleo-Pacific Ocean with the Neuquén Basin during the deposition of the Huitrín Formation. b) the non-marine deposition of Rayoso Formation coeval with Colimapu Formation. c) the onset of foreland basin (Albian) with the Diamante Formation deposition (lower interval-107 Ma MDA) coeval with Las Chilcas Formation. d) the Late Cretaceous (Turonian?) reconstruction with the Diamante Formation and BRCU deposition, with the presence of topographic barrier dividing the foreland basin (based on Mescua et al., 2013; Balgord and Carrapa, 2016; Muñoz et al., 2018; Gómez et al., 2019; Tapia et al., 2020; Boyce et al., 2020).

Figure 12. a) Regional DEM with the location of the samples from the Diamante Formation (1 and 2; Balgord and Carrapa, 2016; Gómez et al., 2019) and the Neuquén Group (3 to 6; Tunik et al., 2010; Di Giulio et al., 2012; Fennell et al., 2017; Borghi et al., 2019) in the context of the Neuquén Basin. CF: Cordillera Frontal; CP: Cordillera

Principal; PCN: Precordillera Neuquina; CNP: Cordillera Nordpatagónica. b) Comparative probability density plots (PDPs) of detrital zircon U-Pb ages from the samples indicated in a. Zircons younger than 500 Ma were considered. Colored bars represent provenance signatures and the green vertical line marks the relative predominance of ca.107 Ma detrital zircons.

Tables

Table 1. Description of the samples analysed and the apatite and zircon fission track analytical data.

Table 1

Table 1
Description of the samples analysed and apatite and zircon fission track analytical data

Sample	Latitude (S)	Longitude (W)	Stratigraphic unit	Stratigraphic Age	No. of grains	Spontaneous track density ρ_s x 10^5 tracks/cm^2 (Ns)	Induced track density ρ_i x 10^6 tracks/cm^2 (Ni)	Dosimeter track density $\rho_d \times 10^6$ cm^2 (Nd)	Age (Ma) ± 1σ	P (x^2)	P_1 (%)	P_2 (%)
VLP001	34°39'31.04"	69°41'33.68"	Diamante Fm.	Albian	42 (Ap)	1.601 (242)	1.91 (289)	7.47 (5000)	111.9 ± 13.6	31.13	*x*	*x*
2119	34°39'29.19"	69°42'3.21"	Diamante Fm.	Turonian?	37 (Zr)	96.01 (4778)	11.07 (551)	3.33 (5000)	184.0 ± 13.1	0.75	161.1 ± 16.4 (71%)	265.2 ± 46.5 (29%)

Note. Abbreviations are Ns, total number of spontaneous tracks; Ni and Nd, total numbers of induced and dosimeter tracks; P(x^2), x^2 probability. No confined track lengths were measured. ζ zeta value: 131.3 ± 5.1 (ZFT_2119); 352.4 ± 22.9 (AFT_VLP001). Counted by Dr. Arzadún G. in La.Te. Andes S.A. Etching conditions: 5.5 N (HNO_3) for 20 s at 20°C (AFT_VLP001); NaOH-KOH eutectic solution of 8 g of sodium hydroxide (NaOH) and 11.5 g of potassium hydroxide (KOH), melted at 210°C (ZFT_2119). Dosimeter glasses: IRMM540 (AFT_VLP001) and IRMM541 (ZFT_2119). All samples were irradiated in the RA-3 Reactor in Centro Atómico Ezeiza (Buenos Aires, Argentina). See Appendix 3 for further information.

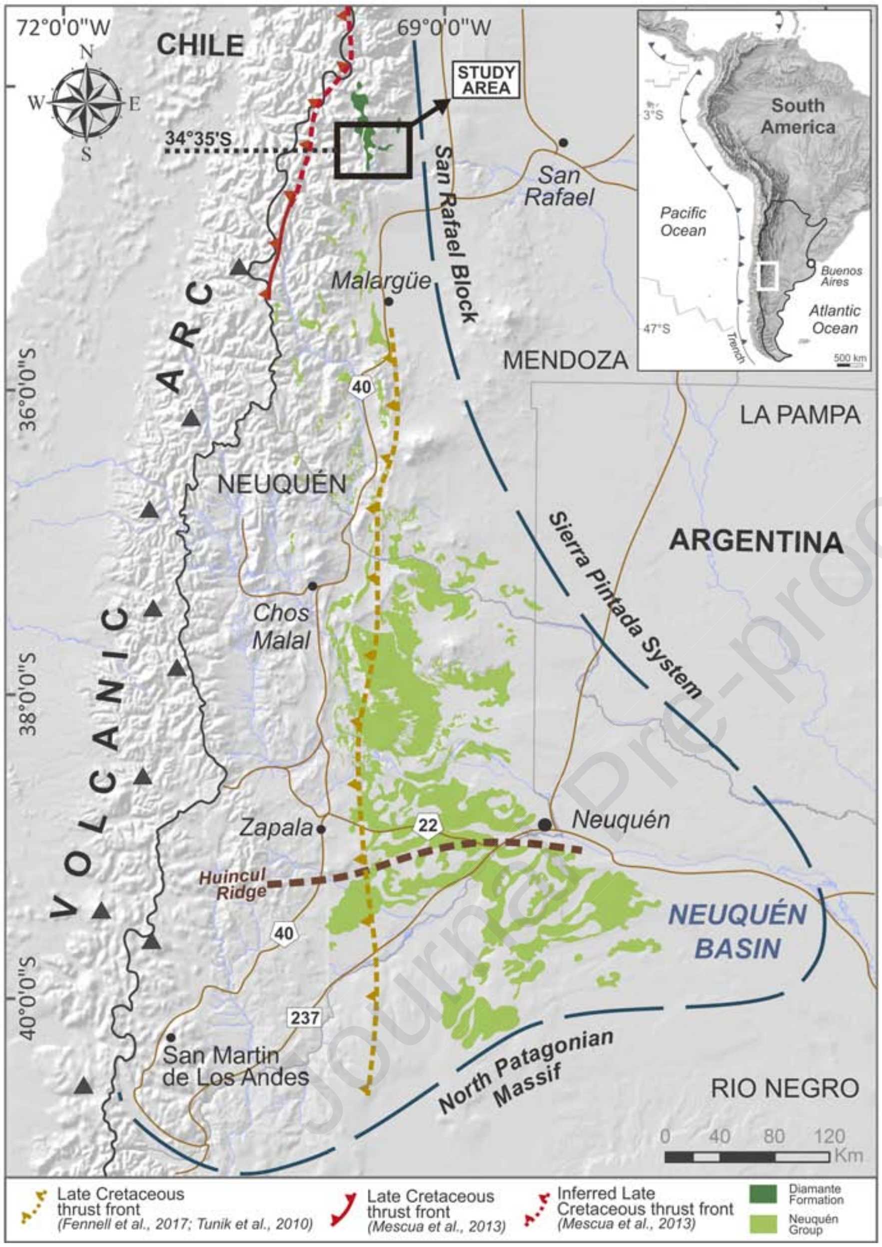

72°0'0"W
69°0'0"W
CHILE
STUDY AREA
34°35'S
San Rafael
San Rafael Block
Malargüe
MENDOZA
LA PAMPA
NEUQUÉN
ARGENTINA
Sierra Pintada System
VOLCANIC ARC
Chos Malal
Zapala
Neuquén
Huincul Ridge
NEUQUÉN BASIN
San Martin de Los Andes
North Patagonian Massif
RIO NEGRO
36°0'0"S
38°0'0"S
40°0'0"S
40
22
237
0 40 80 120 Km
South America
Pacific Ocean
Atlantic Ocean
Buenos Aires
47°S
Trench
500 km
Late Cretaceous thrust front (Fennell et al., 2017; Tunik et al., 2010)
Late Cretaceous thrust front (Mescua et al., 2013)
Inferred Late Cretaceous thrust front (Mescua et al., 2013)
Diamante Formation
Neuquén Group

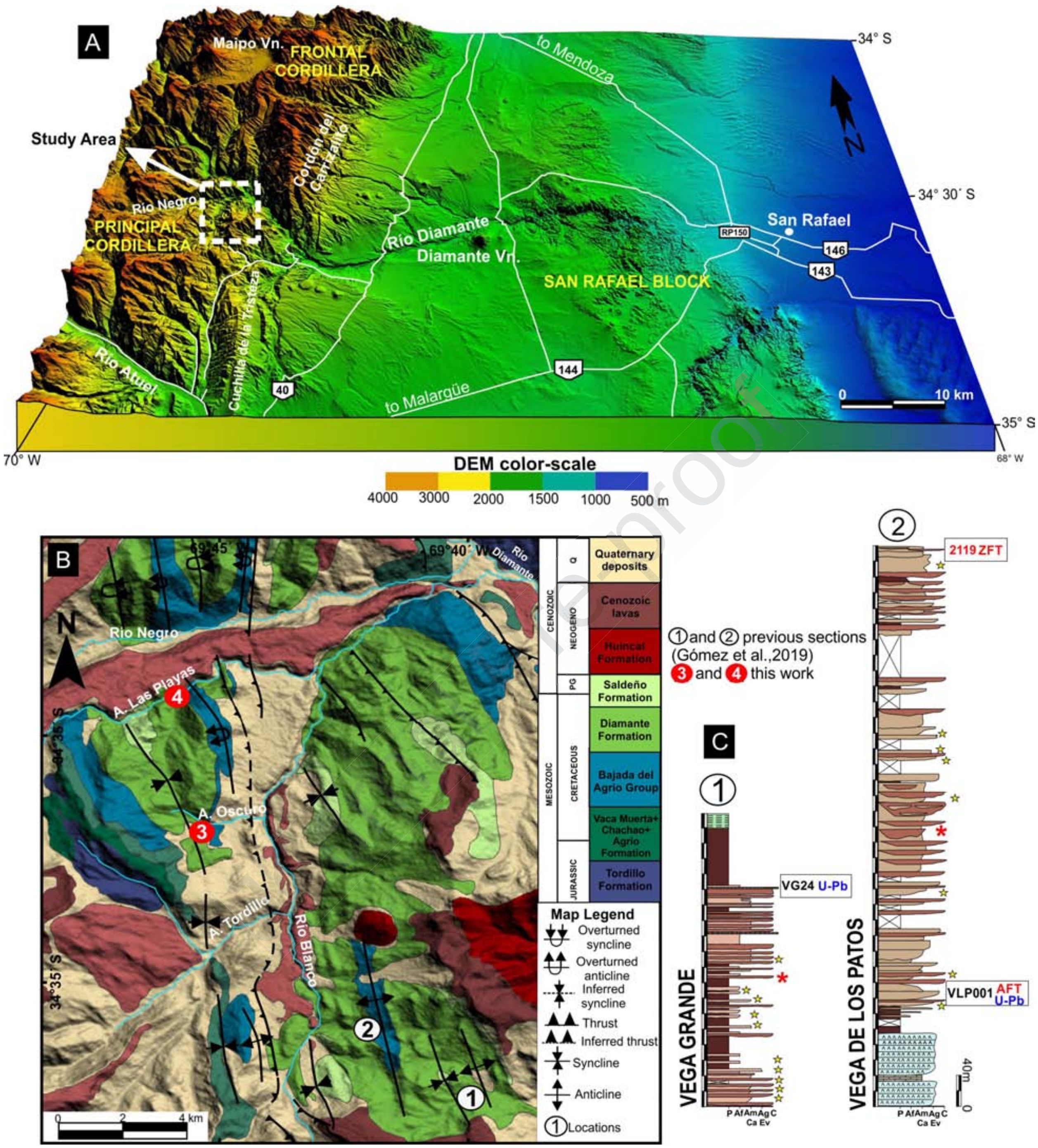
A
Maipo Vn.
FRONTAL CORDILLERA
to Mendoza
34° S
Study Area
Cordón del Carrizalito
Rio Negro
PRINCIPAL CORDILLERA
Río Diamante
Diamante Vn.
34° 30´ S
San Rafael
RP150
146
143
SAN RAFAEL BLOCK
Cuchilla de la Tristeza
Rio Atuel
40
144
to Malargüe
0
10 km
35° S
70° W
68° W
DEM color-scale
4000
3000
2000
1500
1000
500 m
B
69°45´
69°40´ W
Rio Diamante
Rio Negro
A. Las Playas
A. Oscuro
A. Tordillo
Rio Blanco
34°35´S
0
2
4 km
Quaternary deposits
Cenozoic lavas
Huincal Formation
Saldeño Formation
Diamante Formation
Bajada del Agrio Group
Vaca Muerta+ Chachao+ Agrio Formation
Tordillo Formation
CENOZOIC
NEOGENO
PG
MESOZOIC
CRETACEOUS
JURASSIC
Map Legend
Overturned syncline
Overturned anticline
Inferred syncline
Thrust
Inferred thrust
Syncline
Anticline
Locations
1 and 2 previous sections (Gómez et al.,2019)
3 and 4 this work
C
VEGA GRANDE
VG24 U-Pb
VEGA DE LOS PATOS
2119 ZFT
VLP001 AFT U-Pb
40m
0
P AfAmAg C
Ca Ev

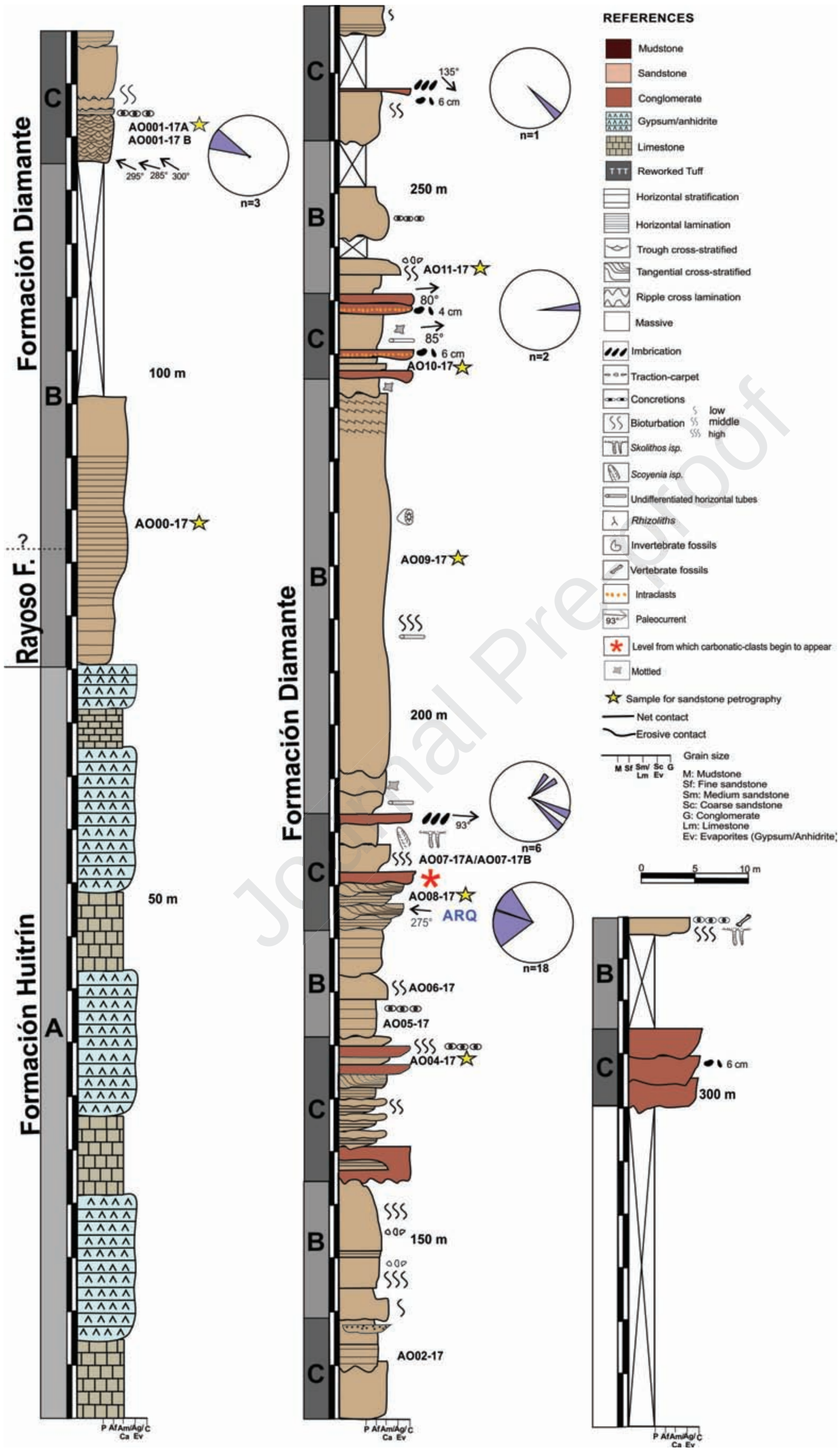
REFERENCES
Mudstone
Sandstone
Conglomerate
Gypsum/anhidrite
Limestone
Reworked Tuff
Horizontal stratification
Horizontal lamination
Trough cross-stratified
Tangential cross-stratified
Ripple cross lamination
Massive
Imbrication
Traction-carpet
Concretions
Bioturbation low middle high
Skolithos isp.
Scoyenia isp.
Undifferentiated horizontal tubes
Rhizoliths
Invertebrate fossils
Vertebrate fossils
Intraclasts
Paleocurrent
Level from which carbonatic-clasts begin to appear
Mottled
Sample for sandstone petrography
Net contact
Erosive contact
Grain size
M: Mudstone
Sf: Fine sandstone
Sm: Medium sandstone
Sc: Coarse sandstone
G: Conglomerate
Lm: Limestone
Ev: Evaporites (Gypsum/Anhidrite)
Formación Diamante
Rayoso F.
Formación Huitrín
Formación Diamante
AO001-17A
AO001-17 B
295° 285° 300°
n=3
100 m
AO00-17
50 m
135°
6 cm
n=1
250 m
AO11-17
80°
4 cm
85°
6 cm
AO10-17
n=2
AO09-17
200 m
93°
n=6
AO07-17A/AO07-17B
AO08-17
275°
ARQ
n=18
AO06-17
AO05-17
AO04-17
150 m
AO02-17
6 cm
300 m
0 5 10 m
A
B
C
P Af Am Ag C
Ca Ev

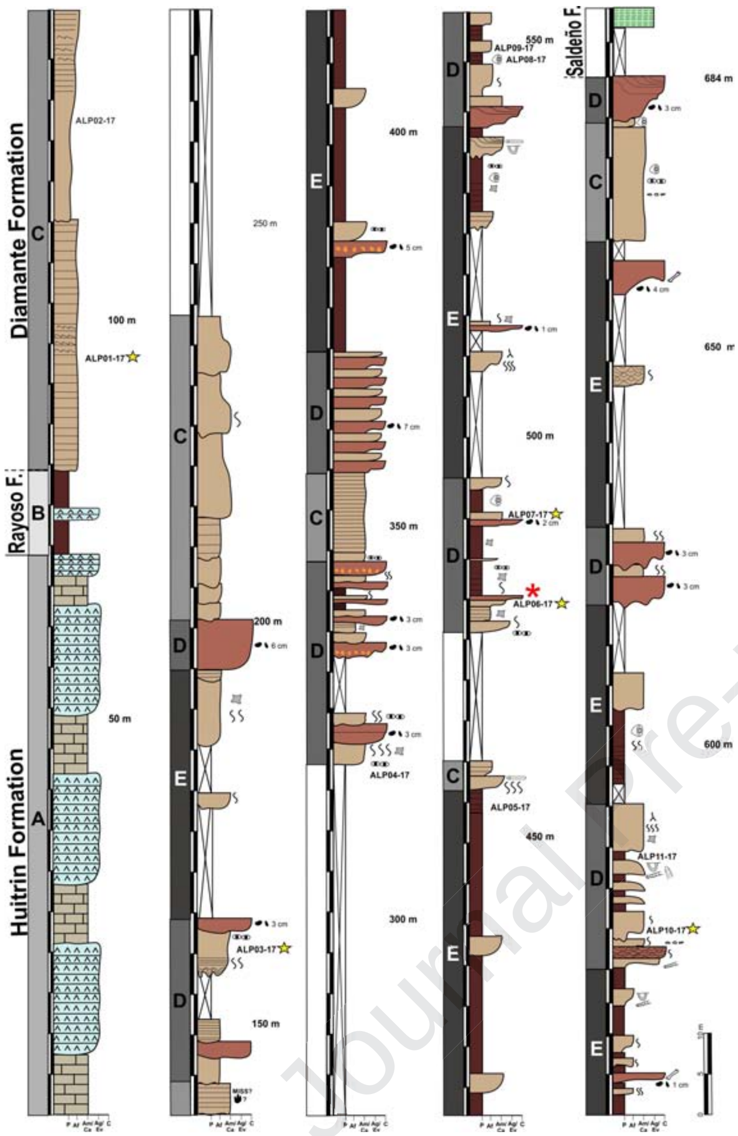
Diamante Formation
Rayoso F.
Huitrin Formation
Saldeño F.
ALP01-17
ALP02-17
ALP03-17
ALP04-17
ALP05-17
ALP06-17
ALP07-17
ALP08-17
ALP09-17
ALP10-17
ALP11-17
50 m
100 m
150 m
200 m
250 m
300 m
350 m
400 m
450 m
500 m
550 m
600 m
650 m
684 m

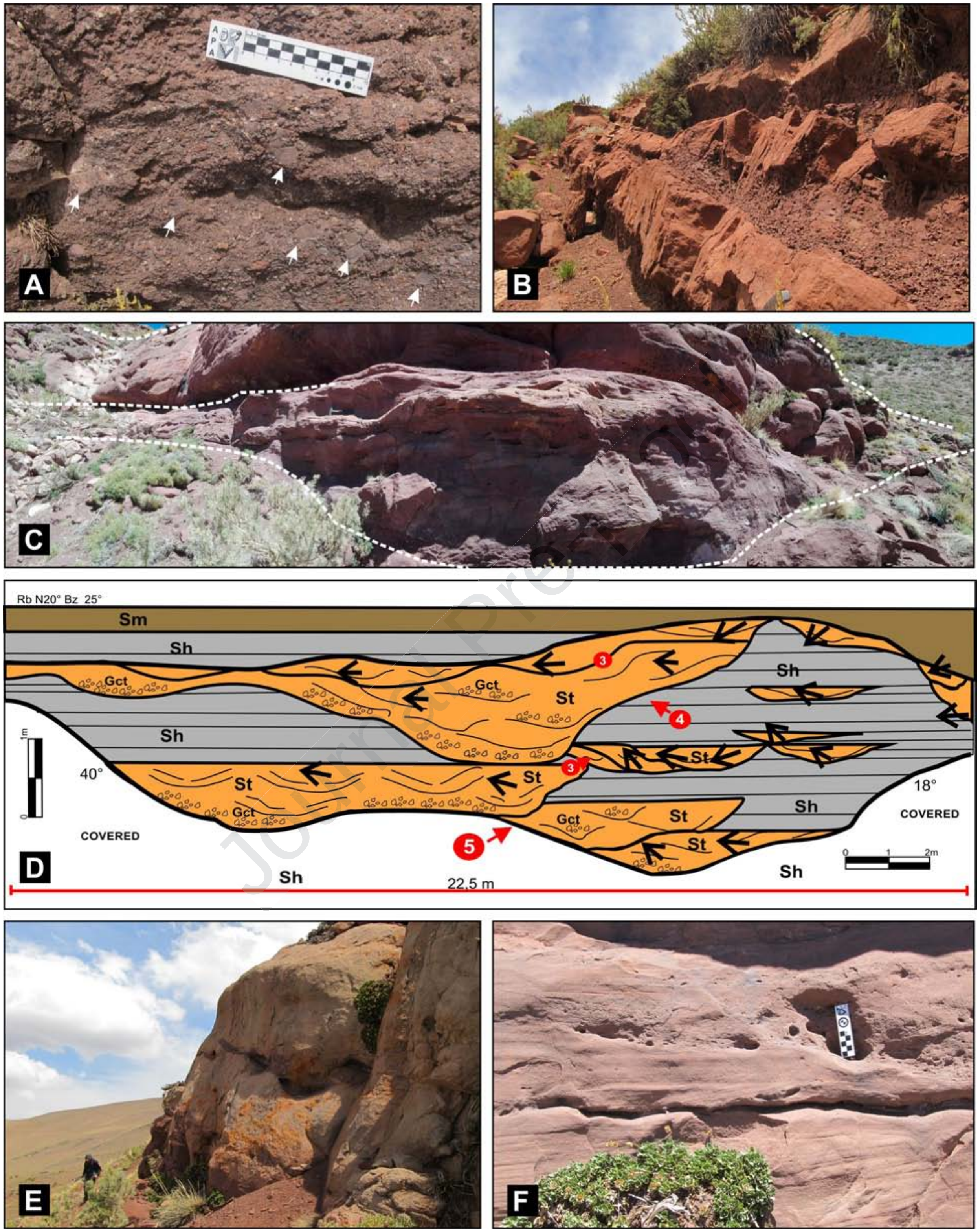
A
B
C
Rb N20° Bz 25°
Sm
Sh
Gct
St
3
4
5
40°
18°
COVERED
22,5 m
D
E
F

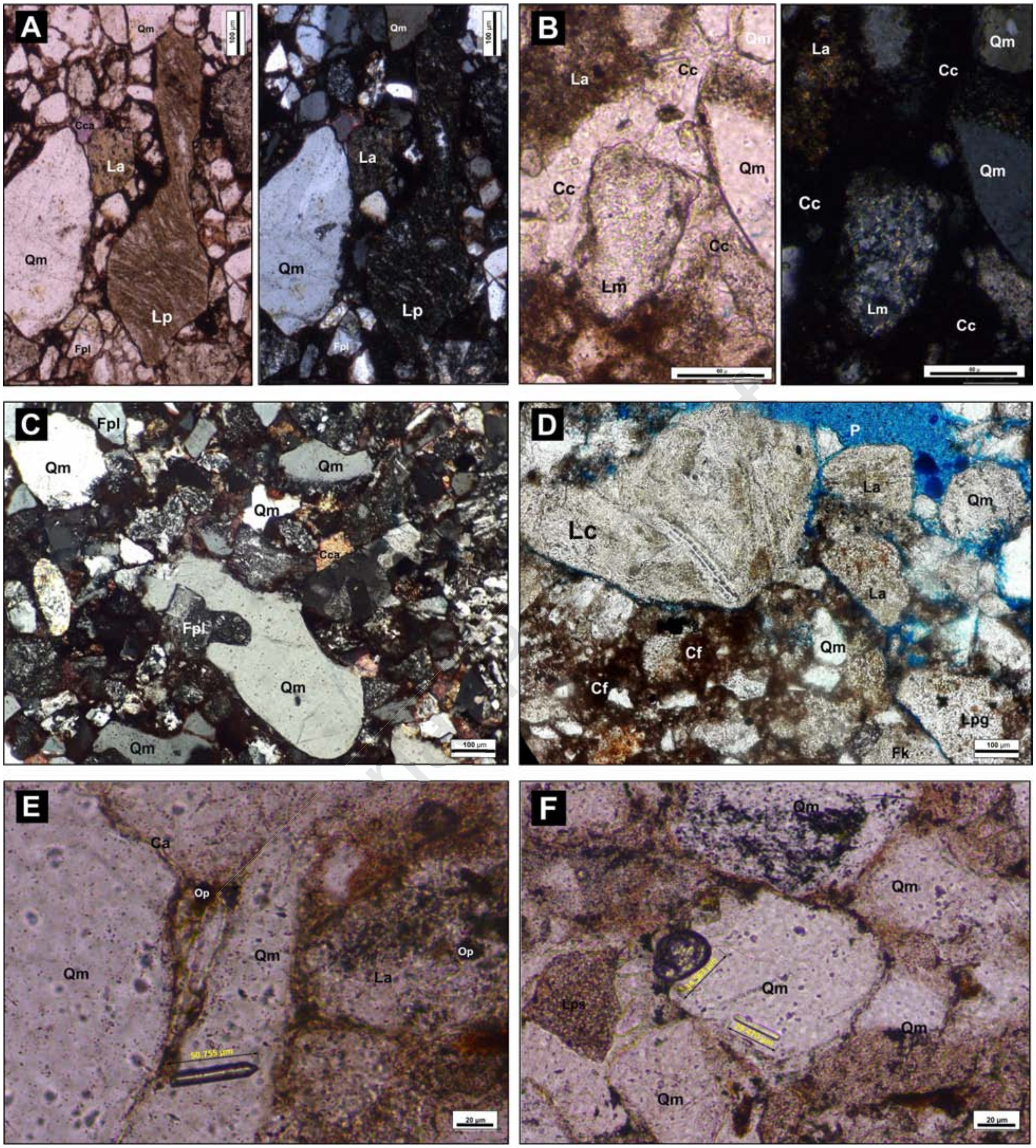
A
Qm
Cca
La
Qm
Lp
Fpl
100 µm
B
La
Cc
Qm
Lm
C
Fpl
Qm
Cca
D
P
Lc
La
Cf
Lpg
Fk
100 µm
E
Ca
Op
La
50.755 µm
20 µm
F
Lps
20 µm

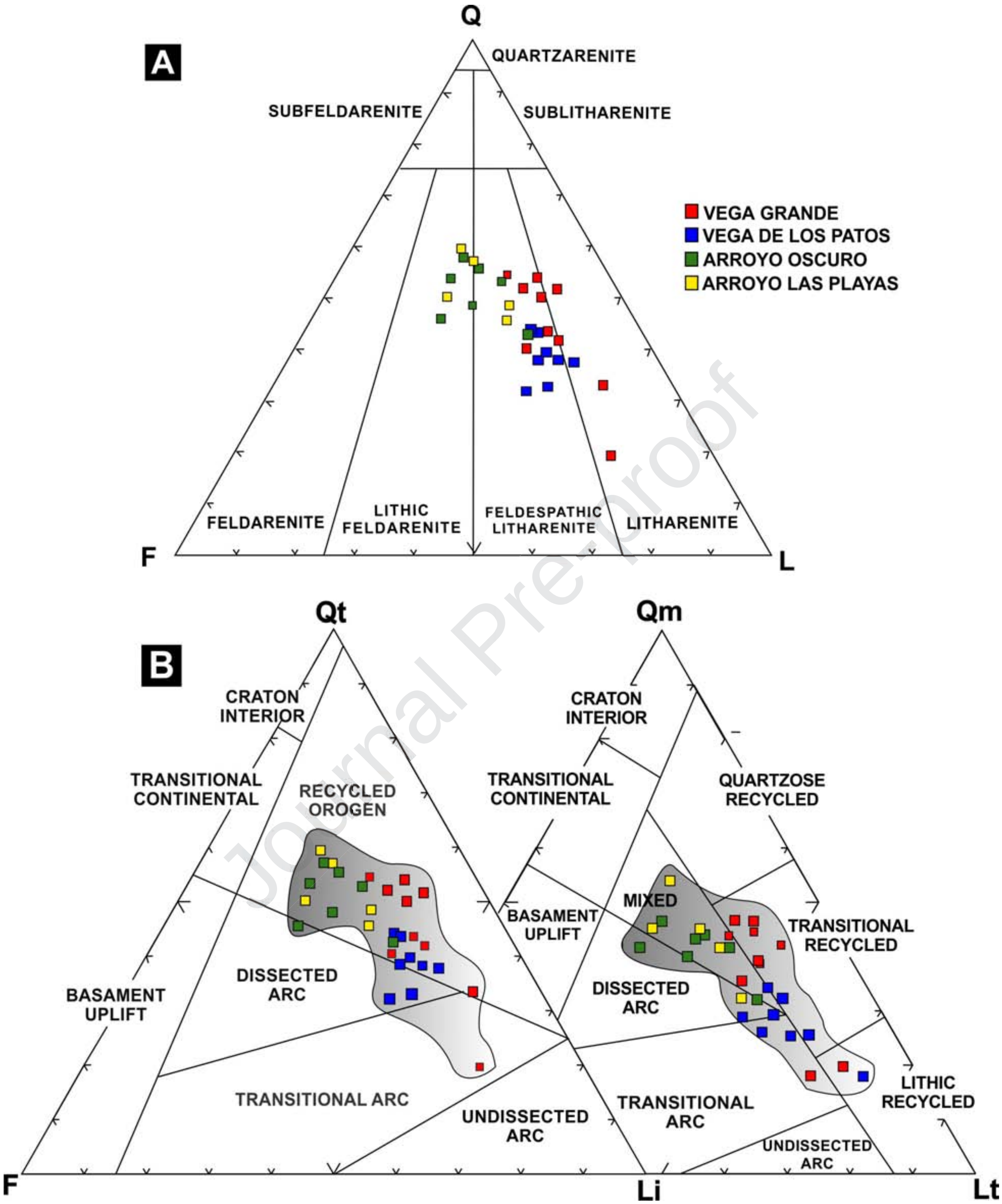
A
Q
QUARTZARENITE
SUBFELDARENITE
SUBLITHARENITE
FELDARENITE
LITHIC FELDARENITE
FELDESPATHIC LITHARENITE
LITHARENITE
F
L
VEGA GRANDE
VEGA DE LOS PATOS
ARROYO OSCURO
ARROYO LAS PLAYAS
B
Qt
CRATON INTERIOR
TRANSITIONAL CONTINENTAL
RECYCLED OROGEN
BASAMENT UPLIFT
DISSECTED ARC
TRANSITIONAL ARC
UNDISSECTED ARC
F
Li
Qm
CRATON INTERIOR
TRANSITIONAL CONTINENTAL
QUARTZOSE RECYCLED
MIXED
BASAMENT UPLIFT
TRANSITIONAL RECYCLED
DISSECTED ARC
TRANSITIONAL ARC
LITHIC RECYCLED
UNDISSECTED ARC
Lt

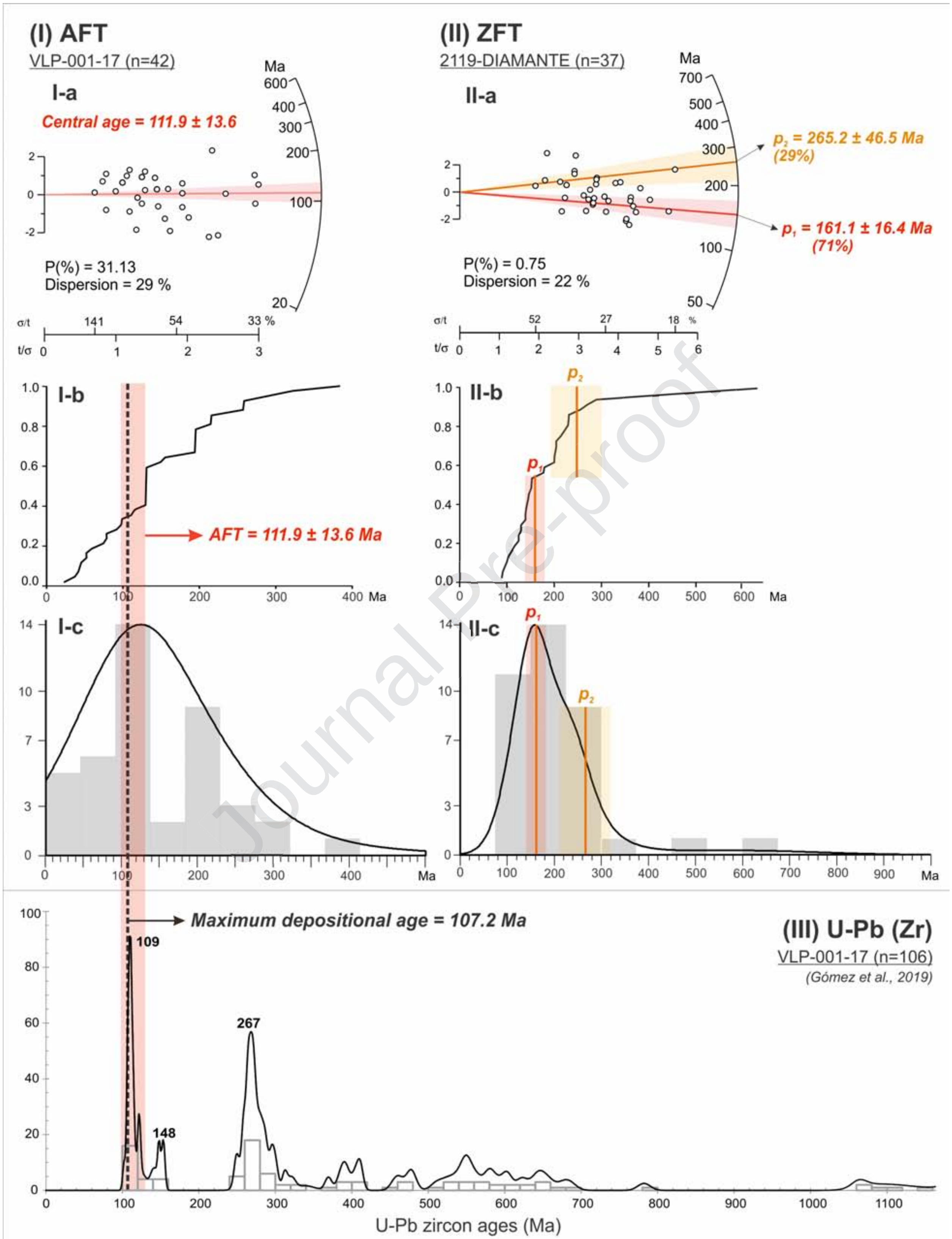

(I) AFT
VLP-001-17 (n=42)
I-a
Central age = 111.9 ± 13.6
P(%) = 31.13
Dispersion = 29 %
I-b
AFT = 111.9 ± 13.6 Ma
I-c
(II) ZFT
2119-DIAMANTE (n=37)
II-a
p2 = 265.2 ± 46.5 Ma (29%)
p1 = 161.1 ± 16.4 Ma (71%)
P(%) = 0.75
Dispersion = 22 %
II-b
II-c
Maximum depositional age = 107.2 Ma
(III) U-Pb (Zr)
VLP-001-17 (n=106)
(Gómez et al., 2019)
109
148
267
U-Pb zircon ages (Ma)

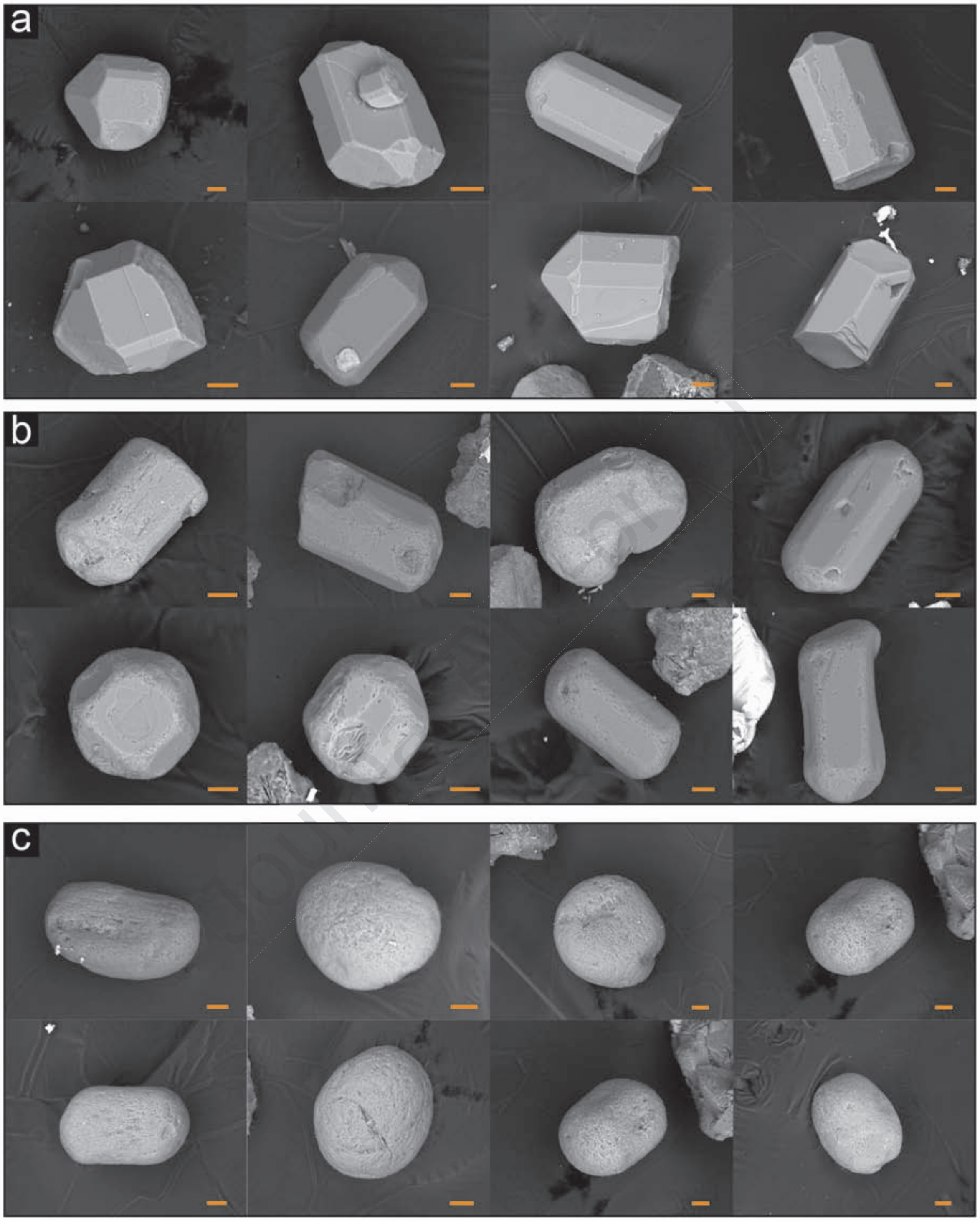
a
b
c

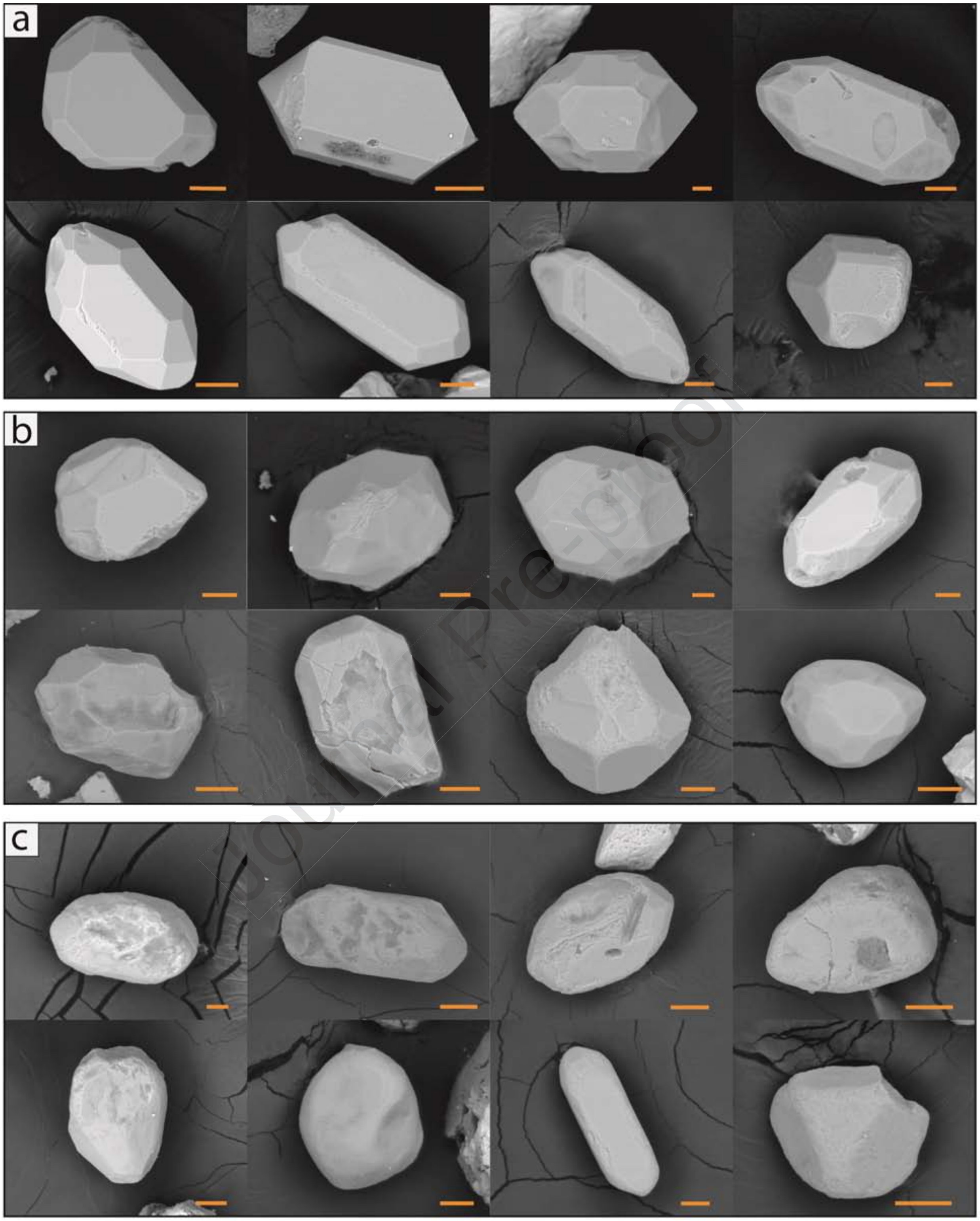
a
b
c

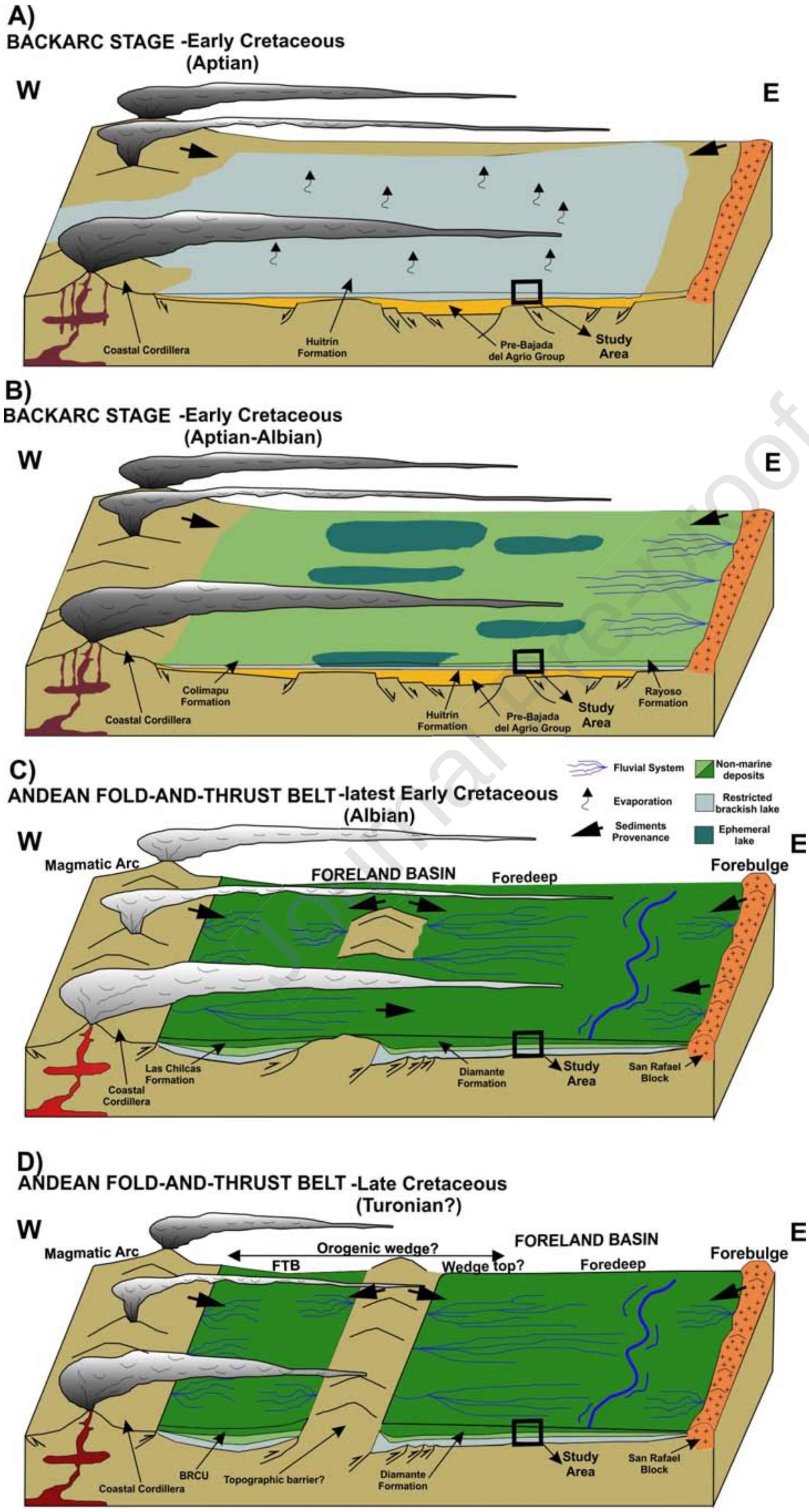
A)
BACKARC STAGE -Early Cretaceous
(Aptian)
W
E
Coastal Cordillera
Huitrin Formation
Pre-Bajada del Agrio Group
Study Area
B)
BACKARC STAGE -Early Cretaceous
(Aptian-Albian)
W
E
Colimapu Formation
Coastal Cordillera
Huitrin Formation
Pre-Bajada del Agrio Group
Study Area
Rayoso Formation
C)
ANDEAN FOLD-AND-THRUST BELT -latest Early Cretaceous
(Albian)
Fluvial System
Non-marine deposits
Evaporation
Restricted brackish lake
Sediments Provenance
Ephemeral lake
W
E
Magmatic Arc
FORELAND BASIN
Foredeep
Forebulge
Las Chilcas Formation
Coastal Cordillera
Diamante Formation
Study Area
San Rafael Block
D)
ANDEAN FOLD-AND-THRUST BELT -Late Cretaceous
(Turonian?)
W
E
Magmatic Arc
Orogenic wedge?
FTB
Wedge top?
FORELAND BASIN
Foredeep
Forebulge
BRCU
Coastal Cordillera
Topographic barrier?
Diamante Formation
Study Area
San Rafael Block

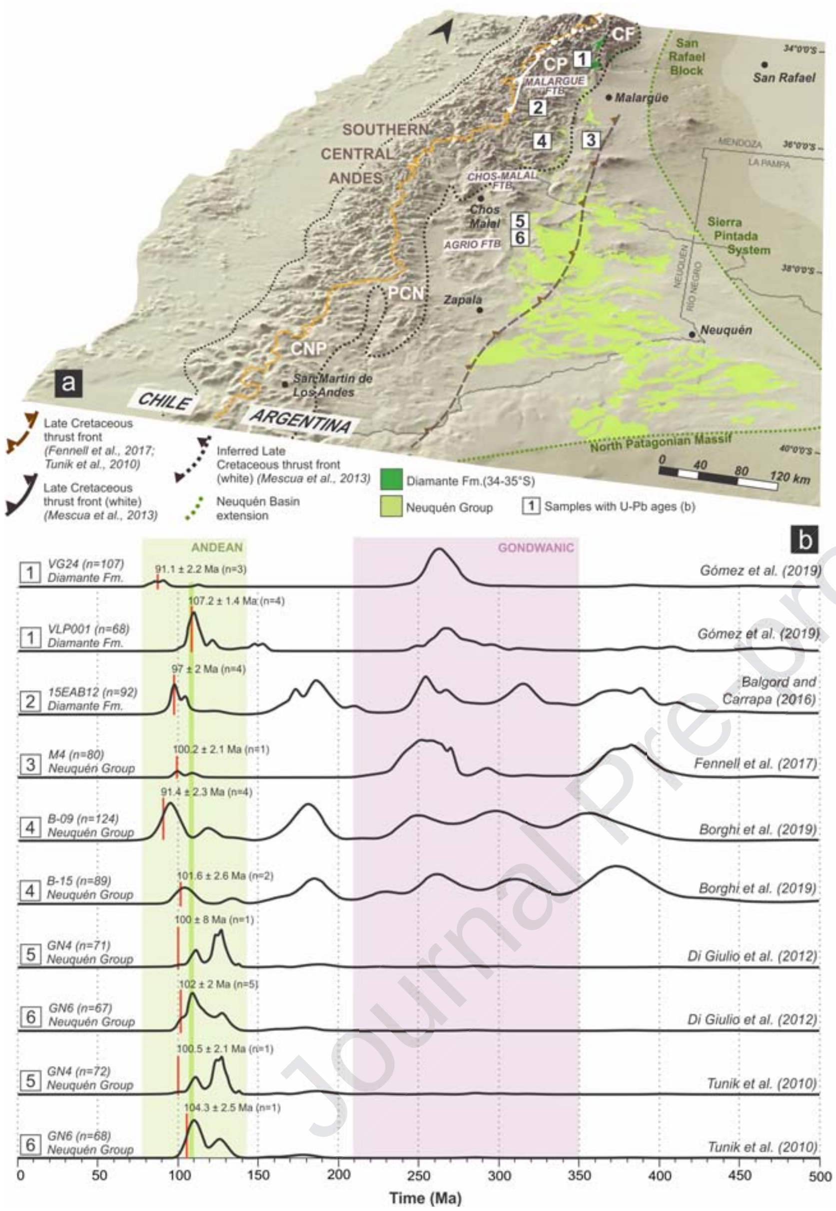
CF
CP
1
MALARGUE FTB
2
4
3
San Rafael Block
San Rafael
Malargüe
SOUTHERN CENTRAL ANDES
CHOS-MALAL FTB
Chos Malal
5
6
AGRIO FTB
Sierra Pintada System
MENDOZA
LA PAMPA
NEUQUEN
RIO NEGRO
PCN
Zapala
Neuquén
CNP
San Martin de Los Andes
a
CHILE
ARGENTINA
North Patagonian Massif
34°0'0"S
36°0'0"S
38°0'0"S
40°0'0"S
0 40 80 120 km
Late Cretaceous thrust front (Fennell et al., 2017; Tunik et al., 2010)
Late Cretaceous thrust front (white) (Mescua et al., 2013)
Inferred Late Cretaceous thrust front (white) (Mescua et al., 2013)
Neuquén Basin extension
Diamante Fm.(34-35°S)
Neuquén Group
1 Samples with U-Pb ages (b)
b
ANDEAN
GONDWANIC
1 VG24 (n=107) Diamante Fm.
91.1 ± 2.2 Ma (n=3)
Gómez et al. (2019)
1 VLP001 (n=68) Diamante Fm.
107.2 ± 1.4 Ma (n=4)
Gómez et al. (2019)
2 15EAB12 (n=92) Diamante Fm.
97 ± 2 Ma (n=4)
Balgord and Carrapa (2016)
3 M4 (n=80) Neuquén Group
100.2 ± 2.1 Ma (n=1)
Fennell et al. (2017)
4 B-09 (n=124) Neuquén Group
91.4 ± 2.3 Ma (n=4)
Borghi et al. (2019)
4 B-15 (n=89) Neuquén Group
101.6 ± 2.6 Ma (n=2)
Borghi et al. (2019)
5 GN4 (n=71) Neuquén Group
100 ± 8 Ma (n=1)
Di Giulio et al. (2012)
6 GN6 (n=67) Neuquén Group
102 ± 2 Ma (n=5)
Di Giulio et al. (2012)
5 GN4 (n=72) Neuquén Group
100.5 ± 2.1 Ma (n=1)
Tunik et al. (2010)
6 GN6 (n=68) Neuquén Group
104.3 ± 2.5 Ma (n=1)
Tunik et al. (2010)
0 50 100 150 200 250 300 350 400 450 500
Time (Ma)

HIGHLIGHTS

- A multiproxy provenance analysis was applied to the Diamante Formation in the northern Neuquén Basin.
- Apatite Fission Track analysis of the Diamante Formation reveals an Albian rapid cooling for its provenance-source.
- A lag time of 3 ma. for the Diamante Formation suggests a volcanic arc provenance during Albian times.
- Diamante Formation records the transition between the backarc and the foreland basin.
- Diamante Formation at 34-35°S was deposited in a foredeep depozone through a Distributive Fluvial System.

Declaration of interests

☒ The authors declare that they have no known competing financial interests or personal relationships that could have appeared to influence the work reported in this paper.

☐The authors declare the following financial interests/personal relationships which may be considered as potential competing interests: